# Ash aggregate-rich pyroclastic density currents of the 431 CE Tierra Blanca Joven eruption, Ilopango caldera, El Salvador

Richard J. Brown[1], Alexa R. Van Eaton[2], Walter Hernández[3], Pearce Condren[1], Clare Sweeney[1], Pierre-Yves Tournigand[4], James W. Vallance[2]

[1]Department of Earth Sciences, University of Durham, Durham, DH1 3LE, UK

[2]U.S. Geological Survey, Cascades Volcano Observatory, Vancouver, Washington 98683 USA

[3]Consultant for: Ministerio de Ambiente y Recursos Naturales, San Salvador, El Salvador

[4]Physical Geography (FARD), Department of Geography, Vrije Universiteit Brussel, Brussels, Belgium

Corresponding author: Richard.brown3@durham.ac.uk

## Abstract

The VEI 6, Tierra Blanca Joven pyroclastic sequence (30–90 km$^3$ DRE volume), erupted from Ilopango caldera, El Salvador, in 431 CE, is the product of one of the largest eruptions of the last two millennia. The eruption devastated Central America's Mayan civilization. The eruption began with a short-lived phase of ash and pumice fall deposition and transitioned to a 'wet' explosive phase during which pyroclastic density currents flowed >40 km from the caldera. Detailed field and sedimentological analyses are provided for the deposits of ash-aggregate-rich pyroclastic density currents generated during early phases of the eruption. The first phase of pyroclastic density current inundation incinerated forests and deposited up to 30 m of, non-welded, ash-rich ignimbrite in proximal regions, along with ash fall layers of co-ignimbrite origin. Following fallout of a thin layer of pumice and lithic lapilli, a second phase of pyroclastic density current inundation and co-ignimbrite ash fall commenced. A range of ash aggregate types is present in the pyroclastic density current deposits and interbedded co-ignimbrite ash fall layers. Whole and broken concentrically layered ash aggregates (accretionary lapilli) reach >50 vol. % in some horizons within some beds in the pyroclastic density current deposits. The evidence indicates that the ash aggregates grew within overriding co-ignimbrite ash plumes and subsequently fell into ground-hugging currents. Our findings suggest that

the aggregate-rich nature of the pyroclastic density current deposits originated through incorporation of lake water into eruptive plumes, which in turn triggered rapid, pervasive aggregation within ash clouds and co-ignimbrite plumes.

**Keywords:** Explosive eruption; volcanic ash aggregation; Ilopango volcano; pyroclastic density currents; accretionary lapilli

## 1. Introduction

Explosive eruptions through caldera lakes can result in the entrainment of large amounts of external water into eruption plumes. The resulting deposits are rich in fine ash, owing to efficient fragmentation coupled with aggregation-enhanced scrubbing of airborne ash (Self and Sparks, 1978; Walker, 1981; Self, 1983; Branney, 1991; Orsi et al., 1992; Wilson, 2001). This water vapour transforms the dynamics of the eruptive plumes by absorbing latent heat during magma-water interaction with evaporation of water, and releasing latent heat during water condensation and ice formation (Koyaguchi and Woods, 1996; Van Eaton et al., 2012a). As a result, water-rich plumes are more prone to partial collapse, leading to complex mixing with ash-rich thermals rising buoyantly from ground-hugging pyroclastic density currents (Van Eaton et al., 2012a). Furthermore, the abundant water promotes ash aggregation, which clumps fine ash into mm- to cm-sized pellets that have higher fall velocities than the dispersed ash component (Schumacher and Schmincke 1991, 1995; Gilbert and Lane, 1994; Brown et al., 2012; Van Eaton et al. 2012b). Studies have demonstrated that aggregation in general terms tends to increase ash fall proximally and reduce it in the distal area (Taddeucci et al., 2011; Van Eaton et al., 2015). Growth of ultrafine ash outer rims can occur when ash aggregates fall through pyroclastic density currents (Brown et al., 2010; Van Eaton and Wilson, 2013). Detailed field studies can help constrain the complex interplay between water involvement, ash aggregation, and the dynamics of ground-hugging currents.

In this paper, we use deposit characteristics to investigate the emplacement of pyroclastic density currents formed during water-rich phases of the 431 CE, dacite-to-rhyolite, Tierra Blanca Joven (TBJ) Plinian eruption at Ilopango caldera, El Salvador, one of the largest eruptions of the last two millennia (Fig. 1: Hart and Steen-McIntyre, 1983; Pedrazzi et al., 2019; Smith et al., 2020). We also discuss the generation of different types of ash aggregates and feedbacks between ash aggregation and the propagation of pyroclastic density currents.

## 2. Geological setting and previous work

Volcanism in Central America is driven by the eastward subduction of the Cocos Plate beneath the Caribbean plate. The resultant Central American Volcanic Arc stretches along most of the west coast from southern Mexico to western Panama (Stoiber and Carr, 1973; Carr et al., 2003). El Salvador is home to numerous arc-related composite volcanoes, dacitic domes, monogenetic volcanic fields, and several silicic calderas, most of which sit in the Median Trough, a Plio-Pleistocene graben (Lexa et al., 2011; Alonso-Henar et al., 2015). Ilopango caldera, in central El Salvador (Fig. 1), an active volcano situated <10 km from the city of San Salvador, home to ~3 million people, is a ~10 × 7 km, flooded caldera with a lake level at 440 m above sea level. The lake holds ~12 $km^3$ of water (Sánchez-Esquival, 2016). The southern wall of the caldera is 200–300 m higher than the north and is part of the upthrown Balsam Mountains that form the southern margin of the median trough (Fig. 1). The volcano has seen at least four ignimbrite-forming eruptions in the past 57 ka, informally named Tierra Blanca 1–4 (Rose et al., 1999; Suñe-Puchol et al., 2019a, 2019b; Jicha and Hernández, 2021). Ilopango caldera also has erupted numerous andesite to dacite lava domes, both inside and outside the caldera (Hernández et al., 2019). The last eruption occurred in 1879–1880 CE, emplacing a subaqueous lava dome that now forms small islands in the SW of the lake (Islotes los Quemados: Golombek et al., 1978; Mann et al., 2004; Richer et al., 2004).

The youngest of the ignimbrite-forming eruptions, and the subject of this study, is the Tierra Blanca 1 event, more widely labelled the Tierra Blanca Joven (TBJ), translating to "young white earth" (Hart and Steen-McIntyre, 1983; Dull et al., 2019; Pedrazzi et al., 2019). The eruption deposited at least 30 cm of ash across almost all of present-day El Salvador, and ash is widely dispersed across Central America and beyond. Meyer-Abich, 1956; Mehringer et al. 2005; Kutterolf et al., 2008a, b; Pedrazzi et al., 2019; Smith et al., 2020). The eruption caused widespread disruption and hardship across the region (Sheets, 1984, 2004; Dull, 2001; Hernández et al., 2015).

Within the TBJ deposits, seven units have been recognised, termed A-G, related to six eruptive phases (Fig. 2; Hart and Steens-McIntyre, 1983). The earliest deposits (units A and B) are two thin, ash and lapilli beds originating primarily as fall deposits with minor pyroclastic density current deposits, which are widely dispersed across the region (Pedrazzi et al., 2019). Units C and D, the focus of this study, are well-preserved, ash aggregate-rich, non-welded pyroclastic density current deposits and ash fall deposits with bulk volumes of ~0.7 and ~5 km$^3$, respectively (Pedrazzi et al., 2019). In proximal areas units C and D are overlain by a metre-thick sequence of parallel-stratified and bedded lapilli fall layers (unit E). The youngest phase produced unit F, a voluminous ignimbrite with lithic-rich lenses, accretionary lapilli-rich facies, and intercalated ash pellet co-ignimbrite fall layers (Pedrazzi et al., 2019; Fig. 2d). Pedrazzi et al. (2019) refer to a widespread fall deposit, coeval with unit F, as a distinct unit (G), which is voluminous (~20 km$^3$ bulk) but poorly preserved in proximal areas. During the eruption, ignimbrite accumulated in the San Salvador basin west of the caldera to form a distinct plateau surface on which the capital city now stands. Modelling of tephra dispersal during the eruption suggests that ash-fall deposits >0.5 cm thick accumulated over an area of $>2 \times 10^6$ km$^2$ during a period of a few days. Much of this ash was dispersed during phases F–G by co-ignimbrite plumes (Pedrazzi et al., 2019). Traces of TBJ ash have been identified >7,000 km away in a Greenland ice core (Smith et al., 2020).

## 3. Methodology

Fieldwork was conducted over three seasons and involved detailed centimetre-scale description and logging of TBJ units C and D at 60 locations around the caldera (Fig. 1). Most measured sections were road cuts, building sites, riverbanks, or cliffs. Latitude and longitude for measured localities are given in Electronic Supplementary File 1. Material at exposures that were suitably damp was carved into coherent, brick-sized monoliths and wrapped in plastic film for transport. The monoliths were air-dried in the laboratory and then blasted with compressed air to reveal the aggregate structures prior to being photographed and subsampled. Grainsize analysis of 30 bulk representative samples of the full lithological spectrum recognised in the field was done by hand sieving the >1 mm fraction at 1 Phi intervals and by laser diffraction on the <1 mm fraction using a Malvern Mastersizer at Cambridge University and are given as volume %. Care was taken to avoid breakage of whole and fragmented ash aggregates in samples. Results from the laser diffraction analysis were converted into weight % using a constant clast density to produce complete grainsize distributions. An additional 61 samples of very fine ash from unit D (representing bulk deposit, whole ash aggregates, cores, and rims) were analysed by laser diffraction at the U.S. Geological Survey in Flagstaff, Arizona, using a Beckman Coulter LS 13 320. Folk and Ward (1957) grain size statistics (sorting, $\sigma_i$ and median diameter, $M_z$) were calculated using Gradistat v. 9.1. Standards and repeat samples were run to establish reproducibility. Representative samples were chosen for componentry analysis and for textural characterisation using optical and scanning electron microscopy.

Table 1 distinguishes the key lithofacies of these units based on the field characteristics, componentry data, and grainsize analyses. We distinguish three main types of ash aggregates: ash clusters (CP1 aggregates of Brown et al., 2012); poorly structured or massive ash pellets (AP1); and accretionary lapilli with well-defined concentric structures (AP2). Additional descriptors are used to delineate the aggregate types in further detail (cf. Table 1 of Van Eaton and Wilson, 2013.

## 4. Units C and D pyroclastic deposits

Units C and D crop out over >2000 km$^2$ and extend to >40 km from the caldera. When deposit thicknesses are plotted against distance from the centre of the caldera, three regions can be broadly defined (Figs 1, 3a): (1) proximal (<10 km), medial (10–25 km), and distal (>25 km) zones. Large fluctuations in the thickness of units C and D characterise proximal zones primarily because of marked topography around the caldera. Distal zone deposits are typically <0.5 m thick (Fig. 3a) and poorly preserved owing to erosion and bioturbation. In most proximal and medial locations, units C and D are texturally and visually distinct. Unit C is generally distinguished from unit D by a coarser-grained, ash matrix, and by elevated abundances of pumice and lithic lapilli. At all studied outcrops the deposits are unconsolidated or weakly consolidated and disaggregate readily on drying.

### 4.1. Unit C pyroclastic density current deposits

Unit C is a widely dispersed sequence of grey to yellow pyroclastic deposits (Fig. 4). At most locations, unit C conformably overlies unit B but in some proximal locations the lower contact of unit C is erosional and unit B is absent. Unit C thins by three orders of magnitude from >30–0.03 m over a distance of ~25 km from the centre of the caldera (Fig. 3a). There is no evidence for erosion of unit C and we infer that the thinning is the result of primary depositional factors. In the proximal zone, unit C varies from 0.5–>30 m thick. The thickest sections crop out along valleys that drain away from the caldera, but one of the thickest measured sections is exposed on the southern caldera wall (locality 35, Fig. 1). The base of the unit is commonly not exposed at localities where it is thickest (e.g., along the northwest margin of the caldera). Thicknesses in the medial zone vary from 0.1–>6 m. Northwest of the caldera, unit C crops out along ridges and valleys. At distal localities, unit C is commonly <0.1 m thick, and is preserved at elevations as high as 1260 m above present caldera lake level (on the eastern flanks of Volcán San Salvador, Fig. 1). The thinning with distance of unit C results from decreases in the number and thickness of beds (Fig. 3a). The 1 m isopach covers ~1000 km$^2$ (Fig. 1). The maximum size of pumice clasts within unit C decreases from 80 mm to 20 mm over a radial distance of ~20 km (Fig. 3c).

In proximal locations, unit C comprises predominantly of beds of massive and stratified ash (lithofacies mA and sA, Table 1; Figs 4 and 5). These are poorly sorted mixtures of ash, pumice and lithic lapilli and accretionary lapilli (Fig. 4). Pumice lapilli account for 1–5 wt. %, and lithic clasts for 5–10 wt. % of samples from this material (see also Pedrazzi et al., 2019). The lithic clast population includes conspicuous orange and red-stained hydrothermally-altered clasts. At two locations (1 and 4, Fig. 5), lower parts of unit C include a succession of massive beds decimetres to >10 metres thick, alternating with stratified ash beds, each up to decimetres thick. Massive beds are ungraded, have sharp, erosive bases and some exhibit slight variations in the abundance of lithic and pumice clasts . In any one vertical section, lower parts of unit C are typically massive and upper beds are increasingly stratified and cross-stratified composed of lapilli-ash (xsLA, Table 1; Fig. 5). Stratified beds may display climbing dune bedforms and regressive bedforms with amplitudes of <0.5–1 m and wavelengths of <5 m (Fig. 4b, d). Foreset dips indicate transport directions away from the caldera and along valley drainages. At several proximal localities (e.g., locality 4, Fig. 1) unit C contains carbonised vegetation, either as flakes dispersed through the matrix or in layers, or as carbonised logs and branches up to 15 cm in diameter. Elutriation pipes rise from some logs.

The upper ~1–10 m of unit C at several proximal outcrops contains matrix to clast-supported accretionary lapilli (lithofacies mAccA and cAcca, Table 1; Figs 4c, e, and 5). These reach 1.5 cm in diameter and are composed of massive, coarser-grained ash cores surrounded by multiple concentric layers of texturally distinct ash (Fig. 4c and e). The outer layer is composed of extremely fine-grained (<10 µm) ash. Fragments of accretionary lapilli are common in the matrix of the ignimbrites. Several localities (11 and 35) exhibit alternating massive 10–150 cm thick beds, and thinner (10–30 cm) cross-stratified beds (Fig. 5). Two thin beds of clast-supported ash pellets occur in unit C at locality 35 along the southern caldera wall (Fig. 5).

In medial localities, unit C is lithologically variable, but is generally composed of beds of massive accretionary lapilli-bearing ash (lithofacies maccA and baacA, Table 1), each typically several centimetres to several decimetres thick (Fig. 6). These are interbedded with centimetre-thick beds of stratified ash and clast-supported ash pellets (lithofacies xsA, sA and mpel, Table 1; Fig. 6).

At distal locations unit C is composed of massive, rarely stratified, yellowish, orange or grey fine ash (lithofacies mA, sA, Table 1) with scattered rounded or angular pumice and lithic coarse ash, rare fine lapilli and whole and fragmented accretionary lapilli. Clast-supported ash pellet layers cap the unit in several distal locations (Fig. 6).

The contact between units C and D varies in its distinction. In proximal locations unit C grades upwards into unit D. At many medial and distal locations, in contrast, there is a sharp contact between the two, with notable changes in colour and texture across the contact. At some locations the boundary is marked by a layer of clast-supported ash pellets, or by a thin layer of coarse ash and fine pumice lapilli fall layer one or two grains thick (Figs 4f and 6).

4.2. Unit D pyroclastic density current deposits

Unit D is a sequence of white or beige, vitric ash-rich, bedded pyroclastic density current deposits and intercalated thin ash pellet fall layers (Figs 6 and 7). It was emplaced across topography that had been substantially subdued by unit C, and it shows less extreme variations in thickness (Fig. 3a). In the proximal zone, it varies in thickness from 1.3 to 6 m. In medial outcrops it varies from 0.13 to 3.2 m. It is typically less than 25 cm thick in distal zones (Fig. 3a and 7). The 1 m-isopach covers ~1000 $km^2$ (Fig. 1).

Unit D is finer grained than unit C and comprises intercalated centimetre-decimetre thick beds of matrix- to clast-supported accretionary lapilli-bearing ash (Fig. 7a), massive fine ash, stratified ash, and clast-supported ash pellets (see Table 1; Fig. 7f). Proximal sections are lithologically similar to distal sections (compare Figs 6 and 8), but individual beds cannot be confidentially traced between outcrops over distances of several kilometres or more. In general, individual beds exhibit either sub-parallel boundaries and thicken and thin laterally, or pinch out over distances of a few metres to tens-of-metres (Fig. 7b). Unit D contains very low abundances of pumice and lithic lapilli (<2 wt. %), but contains abundant whole and broken ash aggregates (0–70 wt %). Ash aggregate-bearing lithofacies account for >55 % of the thickness of measured sections in proximal regions and >90 % of distal sections. Beds in unit D are defined primarily by accretionary lapilli abundance or by basal planar scour surfaces (Figs 6 and 7a). At one proximal outcrop (e.g. locality 53; Fig. 1), a 3 m-thick pumice-rich, massive pyroclastic density current deposit with abundant elutriation pipes overlies unit D (Fig. 7c). This deposit is coarser-grained than the underlying accretionary lapilli-bearing pyroclastic density current deposits and contains pumice clasts up to 10 cm in diameter, and lithic clasts up to 1 cm in diameter. This appears restricted to the drainage NW of the caldera.

A range of ash aggregates occur in unit D (Fig. 9). The most common ash aggregates in unit D are complexly-layered accretionary lapilli (Fig. 9b)(Table 1; see Hoult et al., 2022). The aggregates consist of a poorly structured core composed of several layers of texturally distinct ash that vary in terms of grainsize, porosity, or clast fabric. The average maximum size of accretionary lapilli in unit D decreases from 25 mm to 5 mm over 20 km, although the range of accretionary lapilli sizes within beds at any one location varies substantially (<5–25 mm) (Fig. 3b). They occur in variable concentrations, either dispersed through the matrix or in clast-supported lenses and layers (Fig. 7a), along with abundant accretionary fragments (Fig. 9c, d). Diatoms and ash-sized clasts of clay-rich lake sediment are dispersed throughout the ash aggregates (Fig. 9f).

Structurally simpler ash pellets occur clast-supported and partially coalesced in centimetre-thick fall layers (Figs 6, 7f, and 9a) that cap beds deposited by pyroclastic density currents. They typically persist across outcrops, but the absence of marker horizons prevents correlation of individual ash fall layers between exposures (distances of kilometres). Some of these beds contain subspherical vesicles, < 1–5 mm in diameter. At many outcrops unit D contains up to four layers of clast-supported ash pellets (Figs 6 and 8). These layers are more common towards the top of the unit, and most appear to cap beds of massive accretionary-lapilli-bearing ash or massive ash. At several widely dispersed outcrops, the upper 15–20 cm of unit D is composed of thin, commonly parallel-bedded ash beds with varying textural characteristics (Figs 6 and 7e).

An unusual lithofacies is present at some proximal locations (fines-depleted ash with accretionary lapilli, Table 1). It consists of irregular pockets of coarse-grained, lithic and crystal ash enclosed within a fine ash matrix (Fig. 7d). The pockets occur in association with accretionary lapilli. In other beds, the same lithic-crystal ash is distributed in diffuse layers amongst the aggregates.

At distal outcrops, unit D presents as a couplet comprised of a layer of matrix-supported accretionary-lapilli tuff or massive ash overlain by a layer of clast-supported ash pellets (Fig. 6).

4.3. Particle size distributions and componentry

Unit C is a predominantly ash-rich, lapilli-poor deposit (Fig. 10). Median grainsize ($M_z$) varies from 1–4.3 $\phi$ (Fig. 11), bulk deposits are very poorly sorted ($\sigma_i$ = 2–3.6; Fig. 11) and there is little consistent variation in particle size characteristics with distance from the caldera. Lapilli-sized pumice or lithic clasts (>2 mm) are volumetrically minor and account for 1–20 wt % of the deposits, even in proximal deposits (Fig. 10).

Unit D is finer-grained than unit C and has median grainsize values of 2.9–4.9 $\phi$ (Fig. 11). The deposits are very poorly sorted, with $\sigma_i$ values mostly in the range of 2.1–4.1 (Fig. 11). Individual aggregates are finer grained and better sorted than the bulk ignimbrite (Fig. 11). There is little change in grainsize characteristics with distance from the nominal source. Most lapilli-sized clasts in unit D are whole or fragmented accretionary pellet aggregates (Fig. 10b) and they form prominent coarse-tail peaks in bimodal grainsize histograms in beds that contain aggregates (1–26 wt. %; Fig. 10a). The matrix of the pyroclastic density current deposits contains abundant rim fragments of AP2 aggregates, recognizable down to sub-millimetre sizes (Fig. 9c, d), and it is likely that fragmented accretionary lapilli constitute a significant proportion of the ignimbrite matrix. SEM images of thin-sectioned, coherent deposits show that tiny PC1 aggregates (ash clusters), tens to hundreds of microns in diameter, comprise the matrix of some pyroclastic density current beds (Fig. 9e). It is unclear whether these clusters were derived from fragmentation of larger aggregates, or represent primary aggregation of material within the water-vapour-rich pyroclastic density currents. Fig. 12 shows the grain size characteristics of different aggregate-bearing lithofacies within the unit D deposits, ranging from clast-supported ash pellet fall deposits, to matrix-supported accretionary lapilli with ultrafine-grained rims.

## 5. Interpretation and Discussion

### 5.1 Influence of water on the eruption

During the explosive eruption of silicic magmas, large-scale interactions between erupting magma and surface water bodies can result in a number of processes that modify the grain size and nature of pyroclasts and pyroclastic deposits. Explosive expansion of water vapour on mixing with hot erupting jets may result in greater degrees of fragmentation (phreatomagmatic explosions) and produce deposits that are finer-grained than those from dry eruptions (e.g., Self, 1983; Self and Sparks, 1978). Phreatomagmatic explosions occurring prior to magmatic fragmentation can result in the production of dense, blocky ash shards (e.g., Rontongaio ash, Houghton and Wilson, 1989). Incorporation of large volumes of water into buoyant eruption plumes can result in rain-flushing and enhanced aggregation of volcanic ash and fallout of abundant ash aggregates (Walker, 1981). Contact between hot pyroclasts and cold water during shallow subaqueous eruptions can result in the thermal granulation of pyroclast exteriors (Mastin, 2007; Colombier et al. 2019a). The exact mechanisms by which water interacts with erupting jets during Plinian eruptions remains unclear, and likely varies from eruption-to-eruption and varies during an eruption, depending on the mass eruption rate, the location of magma-water interaction (pre- or post-magmatic fragmentation, in or above the conduit) and the vent conditions and geometry (e.g., Aravena et al. 2018).

The deposits of units C and D exhibit characteristics that indicate that water, presumably from the caldera lake, exerted a strong influence on these phases of the eruption. These include 1) an absence of welding in the ignimbrites even in thick proximal sections, consistent with cooling of the erupted mixtures through vaporisation of lake water (although the temperature of the unit C pyroclastic density currents was still sufficient to burn vegetation). 2) Abundant ash aggregates that indicate widespread aggregation and large volumes of water vapour in the ash clouds. 3) The ash-rich nature of the deposits and the paucity of coarse pumice clasts. 4) The presence of diatoms and finely dispersed sediment clasts that indicate incorporation of lake water into the erupting column (e.g., Van Eaton et al., 2013b; Harper et al., 2015). Entrainment of tropospheric water vapour into the plume was probably subordinate to that derived from lake water. Additionally, the grainsize characteristics of the pyroclastic density current deposits overlap with those of similar ash-rich pyroclastic density current deposits from other large-scale wet explosive eruptions such as the Oruanui eruption, Taupo Caldera (Wilson, 2001). Unit D shares lithological similarities to other silicic, ash-rich pyroclastic density current deposits including unit C of the 1875 CE Askja eruption, Iceland (Self and Sparks, 1978; Sparks et al., 1981), ignimbrites of the Pisolitic Tuffs, Colli Albani, Italy (De Rita et al., 2002), unit B of the Kos Plateau Tuff, Greece (Allen et al., 1999), the Brown tuffs, Vulcano, Italy (Lucchi et al., 2021) and parts of the Poris ignimbrite sheet, Tenerife (Brown and Branney, 2004, 2013).

## 5.2 Pyroclastic density current processes

Unit C differs from unit D: it is coarser-grained, has larger abundances of lithic clasts, including hydrothermally altered clasts, lower abundances of ash aggregates, well-developed cross-stratification and dune bedforms. Unit C also contains charcoal and was thus emplaced at temperatures exceeding ~200° C (e.g., Scott and Glasspool, 2005). The absence of charcoal in unit D probably reflects primarily the prior removal, incineration and burial of vegetation by unit C, but the greater abundance of ash aggregates, and the finer-grainsize of the former might also indicate greater interaction of water with the erupting magma resulting in a lower temperature pyroclastic density current. Pedrazzi et al., (2019) proposed that the differences could have resulted from a contribution from groundwater or hydrothermal water-magma interaction during the emplacement of unit C, and predominantly surface water-magma interaction during the emplacement of unit D. A pause between the currents that deposited units C and D is indicated by the presence of a thin layer of angular pumice and lithic lapilli (Fig. 4f), interpreted as pumice fall layer from a buoyant Plinian-type eruption column, or by the presence of a clast-supported ash pellet fall layer. At some locations, the pumice and lithic clasts fell alongside ash pellets from co-ignimbrite ash clouds. Limited data suggest that the eruption plume that shed the pumice and lithic clasts was dispersed to the south, north and west of the caldera. Absence of these fall layers at locations only a few kilometres from where they are present (Fig. 6) could result from erosion by unit D pyroclastic density currents.

The pyroclastic density currents swept out from the caldera, situated at an altitude of ~450 m above sea level, and flowed >40 km from the volcano.. They flowed across a landscape characterised by substantial topography (Fig. 1). Both currents left behind deposits on the 1800 m-high Volcán San Salvador and the 1100 m-high Balsam Mountains (Fig. 1) indicating that the currents were, in places, >1 km thick. The unit C current buried low-lying land, valleys and depressions in proximal regions to thickness of several tens-of-metres, as well as depositing >15 m-thick deposits on the southern caldera wall, at an altitude of 770 m. Unit C is composed of beds (cm to >20 m thick) of massive lithofacies (Table 1) that account for 60–100 % of the unit. These beds record deposition from currents with high particle concentration lower flow boundaries dominated by granular flow or fluid escape processes (e.g., Branney and Kokelaar, 2002;_Sulpizio et al., 2014; Lube et al., 2021): these types of flow boundaries formed in the current irrespective of ground elevation and distance from the vent. Stratified and cross-stratified lithofacies are volumetrically minor, but similarly occur irrespective of ground elevation or distance, and record deposition from flow-boundaries dominated by traction sedimentation (e.g., Branney and Kokelaar, 2002;_Sulpizio et al., 2014). Metre-scale bedforms are restricted to proximal regions. Alternations of massive and stratified lithofacies (e.g., locality 11, Fig. 5) record pulsatory flow-boundary behaviour, or the periodic impingement of turbulent eddies on the aggrading deposit surface. In many distal locations unit C is a thin and simple deposit comprising a thin layer of massive or stratified ash with scattered accretionary lapilli capped by an ash pellet fall layer. We interpret this as brief deposition from a pyroclastic density current and the showering out of aggregates from a co-ignimbrite ash plume, but note that it is difficult to infer depositional process of thin ash deposits, particularly when poorly exposed as most distal outcrops are.

Unit D is composed predominantly of massive beds of ash with variable abundances of ash aggregates interleaved with layers of clast-supported ash pellets. These beds are interpreted in a similar manner to unit C, as a sequence of pyroclastic density current deposits and co-ignimbrite ash pellet fall layers. The flow boundaries of the depositing currents were ash-rich, had high particle concentrations and were dominated by granular flow or fluid escape processes (e.g., Branney and Kokelaar, 2002; Sulpizio et al., 2014; Lube et al., 2020). The presence of multiple ash pellet fall layers that are not traceable between outcrops indicates localised periods of non-deposition from the unit D pyroclastic density current(s) (Fig. 6). Ash pellet fall layers are not present in unit D in proximal locations and it is unclear if unit D was deposited by multiple, ash-rich pyroclastic density currents, or from a single unsteady pyroclastic density current that waxed and waned repeatedly, allowing ash pellets to accumulate in distal and medial locations as it periodically receded towards source.

We infer that accretionary lapilli fell into the unit C and D pyroclastic density currents from suprajacent ash clouds and were transported laterally until conditions in the lower flow boundaries of the currents favoured their deposition (Hoult et al., 2022). Within the currents they would have behaved like other lapilli-sized particles (e.g., pumice and lithic clasts) and were subject to segregation processes acting during transport due to their larger size (e.g., Branney and Kokelaar, 2002; Choux et al., 2004; Baker et al., 2015; Whelley et al., 2017). Accretionary lapilli were either deposited amongst the ash matrix to form matrix-supported accretionary lapilli-bearing lithofacies, or concentrated into clast-supported layers and lenses. The accumulations of accretionary lapilli in units C and D might be somewhat analogous to pumice or lithic lenses and layers found in ignimbrites (e.g., Pittari et al., 2013) that result from segregation processes in the flow boundary zone and act to sort particles according to their aerodynamic properties (e.g., Branney and Kokelaar, 2002; Choux and Druitt, 2002; Choux et al., 2004). Clast-supported accretionary lapilli layers in similar deposits elsewhere (e.g., Oruanui, Taupo caldera, New Zealand) are traceable beyond the limit of the ignimbrite sheet and are interpreted as fall deposits (Wilson 2001; Van Eaton and Wilson, 2013a). Similar beds in unit D do not trace between outcrops (distances of several kilometres) and often thicken and thin or pinch out, suggesting that they were deposited from pyroclastic density currents. To our knowledge, clast-supported accretionary lapilli beds do not occur beyond 40 km from Ilopango caldera.

The fines-depleted ash with accretionary lapilli lithofacies (fdaccA, Table 1), present in some proximal outcrops, and comprising accretionary lapilli in irregularly shaped pods of crystal-lithic ash, is unusual and bears similarities with lithofacies seen in the Oruanui eruption deposits, Taupo caldera, New Zealand (Wilson, 2001). Wilson interpreted it as the result of water vapour-driven flushing of fine ash when hot pyroclastic density current deposits were deposited on top of cool, water-rich aggregate-bearing fall deposits. We speculate a broadly similar process for the unit D lithofacies involving vapour-driven flushing of wet and cool, aggregate-bearing pyroclastic density current deposits by overlying hotter deposits.

The contact between unit D and the overlying unit E, a thick sequence of alternating ash fall layers and pumice fall layers (Pedrazzi et al. 2019), is locally difficult to define and the base of unit E is taken as the base of the first pumice fall layer. The upper 5–10 cm of unit D at a number of localities (e.g., 20, 21 and 26, Fig. 6) is composed of parallel-bedded ash layers, with sharp or gradational boundaries and variable proportions of ash pellets. These may record a gradual transition from pyroclastic density current activity to the unsteady ash and pumice fall activity that characterised unit E.

5.3 Ash aggregate formation and interaction with pyroclastic density currents

The distribution of different types of ash aggregates within units C and D is similar to that seen in pyroclastic density current deposits at other volcanoes (e.g., Brown et al., 2010; Brown et al., 2011; Van Eaton and Wilson, 2013) and we interpret it in a similar manner. Accretionary lapilli are confined to beds deposited by pyroclastic density currents. Ash pellets, in contrast, are restricted to centimetre-thick fall layers and are clast-supported. We infer that ash aggregation initiated within the well-mixed eruption column and in co-ignimbrite ash plumes that rose above the pyroclastic density currents, initially forming ash clusters and ash pellets. These pellets descended through fine-grained co-ignimbrite plumes and the dilute tops of pyroclastic density currents, where changes in ambient conditions (e.g., variations in particle size distributions, temperature, and liquid water availability) resulted in the accretion of texturally distinct concentric layers—particularly the ultrafine outer rims around the accretionary lapilli (see also Brown et al., 2010; Van Eaton and Wilson, 2013). Accretionary lapilli fell into and were transported by the pyroclastic density current before being deposited as outlined above (Hoult et al., 2022). This further establishes a link between pyroclastic density currents and the growth of complex accretionary lapilli with ultrafine-grained rims (Brown et al., 2010; Van Eaton and Wilson, 2013). These aggregates preferentially occur in association with pyroclastic density currents and, alongside other evidence, are useful indicators of the passage of pyroclastic density currents in the absence of other confirmatory evidence. This is potentially useful when investigating past eruptive activity and hazards at volcanoes where exposure of pyroclastic deposits is poor, or where clear evidence for deposition by pyroclastic density currents is lacking.

The particle size distributions of pyroclastic density current deposits are shaped and modified by fragmentation, erosion and attrition processes at the vent and by transport, segregation, attrition, entrainment and deposition processes within pyroclastic density currents (e.g., Sparks and Walker 1977; Macedonio et al., 2014; Branney and Kokelaar, 2002; Dufek and Manga, 2008; Sulpizio et al., 2014; Roche, 2015; Jones and Russell, 2017). The fall-out of ash aggregates from overriding ash clouds can also modify the particle size distribution of pyroclastic density current deposits. Accretionary lapilli abundances (whole and broken) within the TBJ deposits vary from 0–>70 wt. %, however, quantifying the exact contribution of aggregates to the deposits' mass is difficult because the cores of the aggregates are texturally indistinguishable from the matrix in the pyroclastic density current deposits. Even though aggregates can undergo early cementation via salt precipitation on ash particle surfaces (Colombier et al., 2019b) they remain fragile. During transport, comminution of accretionary lapilli would disperse fragments of cores and rims into matrix material and lead to enrichment in fines, indeed, the greatest abundances of accretionary lapilli occur in unit D, which is finer-grained than unit C (Fig. 11). This presents a scenario whereby a pyroclastic density current could become partly self-sustaining. Pyroclastic density currents can continue to flow until they become buoyant through the loss of mass via deposition and elutriation and by entraining and heating the surrounding air. In essence, falling ash aggregates could partly compensate for mass lost via deposition and elutriation, as a portion of the transported mass becomes recycled or added to via aggregation and fallout processes in co-ignimbrite ash clouds or eruption-fed ash clouds.

## 6. Conclusions

Units C and D of the 431 CE Tierra Blanca Joven eruption, Ilopango caldera, El Salvador, were deposited during the early phases of the eruption by pyroclastic density currents that travelled >40 km away from the caldera. The deposits exhibit multiple lines of evidence for interaction between lake water and eruptive jets including an ash-rich nature evident from proximal to distal regions, abundant ash aggregates, cool emplacement temperatures, and presence of diatoms and lake sediments within the deposits. The currents surmounted all regional topography, including the 1700 m-high San Salvador volcano. Unit C incinerated forests and buried proximal regions in ash-rich deposits that exceed several tens-of-metres thick. A thin pumice fall deposit records a brief pause between inundation by units C and D pyroclastic density currents. Unit D, finer-grained and containing abundant ash aggregates, was emplaced across a subdued landscape. Lithofacies analysis of units C and D reveal deposition from unsteady currents (or multiple currents) in which flow boundary zones were mostly characterised by high particle concentrations and dominated by granular flow or fluid escape processes. The resultant deposits are typically massive and bedded. Unit C was locally emplaced from flow boundaries dominated by traction sedimentation. A significant proportion of the mass of unit D deposits is made up of whole and comminuted accretionary lapilli that initially grew in co-ignimbrite plumes and eruption-fed ash clouds and that entered the current as it was moving. Interleaved with the pyroclastic density current deposits are thin, laterally restricted ash pellet fall layers derived from co-ignimbrite ash plumes that record local pauses in current activity. The distribution of different types of ash aggregates throughout units C and D, supports notions of aggregates evolving over time from simple aggregates (ash pellets) to complex aggregates (accretionary lapilli) via growth and transport through eruption plumes, co-ignimbrite plumes and pyroclastic density currents.

**Acknowledgements**

This research was funded by a grant from the National Geographic Committee for Research and Exploration (grant number: GEFNE7-11) awarded to Brown. Van Eaton acknowledges U.S. National Science Foundation grant EAR-1250029. We thank the Ministerio de Ambiente y Recursos Naturales, El Salvador for vehicle and logistical support, and we thank Alex Chavez, Cecilia Polio, Demetrio Escobar, and Carlos Pullinger for field assistance. We thank Bruce Houghton for assistance in the field and for helping introduce Brown and Van Eaton to the TBJ. We thank Chris Rolfe (Cambridge University) for running grainsize analyses, and Leon Bowen for assisting with the use of the SEM. We thank Colin Wilson, Roberto Sulpizio and an anonymous reviewer for their edits and comments that greatly improved the manuscript.

## Disclaimer

Any use of trade, firm, or product names is for descriptive purposes only and does not imply endorsement by the U.S. Government.

## CRediT author statement

**Richard Brown:** conceptualization, funding acquisition, project administration, investigation, writing (original draft). **Alexa R Van Eaton:** conceptualization, investigation, writing (review and editing) **Walter Hernández**: project administration, investigation, writing (review and editing). **Pierre-Yves Tournigand:** investigation, writing (review and editing) **Pearce Condren, Clare Sweeney:** investigation. **James Vallance:** conceptualization **(**writing - review and editing).

## References


Allen, S.R., Cas, R.A.F., 1998. Rhyolitic fallout and pyroclastic density current deposits from a phreatoplinian eruption in the eastern Aegean Sea, Greece. J. Volcanol. Geotherm. Res. 86, 219-251. https://doi.org/10.1016/S0377-0273(98)00080-8

Alonso-Henar, J., Schereurs, G., Martínez-Díaz, J.J., Alvarez-Gómez, J.A., Villamor, P., 2015. Neotectonic development of El Salvador Fault Zone and implication for deformation in Central America Volcanic Arc: Insights from 4-D analog modeling experiments. Tectonics 34, doi:10.1002/2014TC003723

Aravena, A., de' Michieli Vitturi, M., Cioni, R., Neri, A., 2018. Physical constraints for effective magma-water interaction along volcanic conduits during silicic explosive eruptions. Geology 46, 867-870. https://doi.org/10.1130/G45065.1

Branney, M.J., 1991. Eruption and depositional facies of the Whorneyside Tuff Formation, English Lake District: An exceptionally large-magnitude phreatoplinian eruption. Geol. Soc. Am. Bull. 103, 886-897. https://doi.org/10.1130/0016-7606(1991)103<0886:EADFOT>2.3.CO;2

Branney, M.J., Kokelaar, P., 2002. Sedimentation of ignimbrites from pyroclastic density currents: Geol. Soc. Lond Mem. 27.

Brown, R.J., Branney, M.J., 2004. Event-stratigraphy of a caldera-forming ignimbrite eruption on Tenerife: the 273 ka Poris Formation. Bull. Volcanol. 66, 392-416. https://doi.org/10.1007/s00445-003-0321-y

Brown, R.J., Branney, M.J., Maher, C., Davila Harris, P., 2010. Origin of accretionary lapilli within ground-hugging density currents: evidence from pyroclastic couplets on Tenerife. Geol. Soc. Am. Bull. 122, 305-320. https://doi.org/10.1130/B26449.1

Brown, R.J., Bonadonna, C., Durant, A.J., 2012. A review of volcanic ash aggregation. Phys. Chem. Earth 45, 65-78. https://doi.org/10.1016/j.pce.2011.11.001

Brown, R.J., Branney, M.J. (2013). Internal flow variations and diachronous sedimentation within extensive, sustained, density-stratified pyroclastic density currents flowing down gentle slopes, as revealed by the internal architectures of ignimbrites on Tenerife. Bull. Volcanol. 75, ~~1-24~~. https://doi.org/10.1007/s00445-013-0727-0

Carey, S., Sparks, R.S.J., 1986. Quantitative models of the fallout and dispersal of tephra from volcanic eruption columns. Bull. Volcanol. 48, 109-125. https://doi.org/10.1007/BF01046546

Carey, R.J., Houghton, B.F., Thordarson, T., 2009. Abrupt shifts between wet and dry phases of the 1875 eruption of Askja Volcano: microscopic evidence for macroscopic dynamics. J. Volcanol. Geotherm. Res. 184, 256-270. https://doi.org/10.1016/j.jvolgeores.2009.04.003

Carr, M.J., Feigenson, M.D., Patino, L.C. and Walker, J.A., 2003. Volcanism and geochemistry in Central America: Progress and problems. *Geophysical Monograph-American Geophysical Union*, *138*, pp.153-174.

Choux, C. M., & Druitt, T. H. 2002. Analogue study of particle segregation in pyroclastic density currents, with implications for the emplacement mechanisms of large ignimbrites. *Sedimentology*, *49*(5), 907-928. https://doi.org/10.1046/j.1365-3091.2002.00481.x

Choux, C., Druitt, T. and Thomas, N., 2004. Stratification and particle segregation in flowing polydisperse suspensions, with applications to the transport and sedimentation of pyroclastic density currents. *Journal of Volcanology and Geothermal Research*, *138*(3-4), pp.223-241. https://doi.org/10.1016/j.jvolgeores.2004.07.004

Cole, P.D., Scarpati, C., 1993. A facies interpretation of the eruption and emplacement mechanisms of the upper part of the Neapolitan Yellow Tuff, Campi Flegrei, southern Italy. Bull. Volcanol. 55, 311-326. https://doi.org/10.1007/BF00301143

Colombier, M., Scheu, B., Kueppers, U., Cronin, S.J., Mueller, S.B., Hess, K.U., Wadsworth, F.B., Tost, M., Dobson, K.J., Ruthensteiner, B., Dingwell, D.B., 2019a. In situ granulation by thermal stress during subaqueous volcanic eruptions. Geology 47, 179-182. https://doi.org/10.1130/G45503.1

Colombier, M., Mueller, S.B., Kueppers, U., Scheu, B., Delmelle, P., Cimarelli, C., Cronin, S.J., Brown, R.J., Tost, M., Dingwell, D.B., 2019b. Diversity of soluble salt concentrations on volcanic ash aggregates from a variety of eruption types and deposits. Bull. Volcanol., 81, 39. https://doi.org/10.1007/s00445-019-1302-0

De Rita, D., Giordano, G., Esposito, A., Fabbri, M., Rodani, S., 2002. Large volume phreatomagmatic ignimbrites from the Colli Albani Volcano (Middle Pleistocene, Italy). J. Volcanol. Geotherm. Res. 118, 77-98. https://doi.org/10.1016/S0377-0273(02)00251-2

Dufek, J., Manga, M. ,2008. In situ production of ash in pyroclastic flows. J. Geophys. Res. Solid Earth. 113, https://doi.org/10.1029/2007JB005555

Dull, R.A., Southon, J.R., Sheets, P., 2001. Volcanism, ecology and culture: A reassessment of the Volcán Ilopango TBJ eruption in the southern Maya realm. Latin Am. Antiq. 12, 25-44. https://doi.org/10.2307/971755

Dull, R.A., Southon, J.R., Kutterolf, S., Anchukaitis, K.J., Freundt, A., Wahl, D.B., Sheets, P., Amaroli, P., Hernández, W., Wiemann, M.C., Oppenheimer, C., 2019. Radiocarbon and geologic evidence reveal Ilopango volcano as source of the colossal 'mystery' eruption of 539/40 CE. Quat. Sci. Rev. 222, 105855. https://doi.org/10.1016/j.quascirev.2019.07.037

Durant, A.J., Brown, R.J., 2016. Ash aggregation in volcanic clouds. In: Mackie, S., Cashman, K., Ricketts, H, Rust A., Watson, M. (Eds) Volcanic Ash: Hazard observation. Elsevier, Amsterdam, pp. 53-65.

Fauria, K.E., Manga, M., Chamberlain, M., 2016. Effect of particle entrainment on the runout of pyroclastic density currents. J. Geophys. Res. Solid Earth 121, 6445-6461. https://doi.org/10.1002/2016JB013263

Folk, R.L., Ward, W.C., 1957. Brazos River bar: a study in the significance of grain size parameters. J. Sediment. Petrol. 27, 3-26. https://doi.org/10.1306/74D70646-2B21-11D7-8648000102C1865D

Gilbert, J.S., Lane, S.J., 1994. The origin of accretionary lapilli. Bull. Volcanol. 56, 398-411. https://doi.org/10.1007/BF00326465

Golombek, M.P., Carr, M.J., 1978. Tidal triggering of seismic and volcanic phenomena during the 1879-1880 eruption of Islas Quemadas volcano in El Salvador, Central America. J. Volcanol. Geotherm. Res. 3, 299-307. https://doi.org/10.1016/0377-0273(78)90040-9

Harper, M. A., Pledger, S. A., Smith, E. G., Van Eaton, A. R., & Wilson, C. J. (2015). Eruptive and environmental processes recorded by diatoms in volcanically dispersed lake sediments from the Taupo Volcanic Zone, New Zealand. *Journal of paleolimnology*, *54*(4), 263-277.

Hart, W.J.E., Steen-McIntyre, V., 1983. Tierra Blanca Joven tephra from the AD 260 eruption of Ilopango Caldera. In: Sheets, P.D. (Ed), Archaeology and Volcanism in Central America: The Zapotitan Valley of El Salvador. University of Texas Press, Austin, Texas, USA, pp. 14-34.

Hernández, W., Aguirre-Díaz, G., Ayala, P., 2015. La erupción Tierra Blanca Joven y la diáspora de los Mayas. In: Erquicia, J., Shibata, S. (Eds), Museo Nacional de Antropología David J. Guzmán, V Congreso Centroamericano de Arqueología en El Salvador, pp. 227-237.

Hernández, W., Alvarado, G.E., Jicha, B., Mixco, L., 2019. El domo volcánico El Güegüecho (1, 88 Ma) y su evolución en el contexto de la caldera de Ilopango, El Salvador. Rev. Geol. Am. Cent. 60, 41-64. https://doi.org/10.15517/rgac.v2019i60.36462

Hoult, H., Brown, R.J., Van Eaton, A.R., Hernandez, W., Dobson, K.J. and Woodward, B., 2022. Growth of complex volcanic ash aggregates in the Tierra Blanca Joven eruption of Ilopango Caldera, El Salvador. *Journal of Volcanology and Geothermal Research*, *431*, p.107670. https://doi.org/10.1016/j.jvolgeores.2022.107670

Houghton, B.F., Carey, R.J., 2019. Physical constraints for effective magma-water interaction along volcanic conduits during silicic explosive eruptions. Geology 47, e461. https://doi.org/10.1130/G45065.1

Houghton, B.F., Carey, R.J., Cashman, K.V., Wilson, C.J.N., Hobden, B.J., Hammer, J.E.,2010. Diverse patterns of ascent, degassing, and eruption of rhyolite magma during the 1.8 ka Taupo eruption, New Zealand: evidence from clast vesicularity. J. Volcanol. Geotherm. Res. 195, 31-47. https://doi.org/10.1016/j.jvolgeores.2010.06.002

Houghton, B.F. and Wilson, C.J.N., 1989. A vesicularity index for pyroclastic deposits. *Bulletin of volcanology*, *51*(6), pp.451-462. https://doi.org/10.1007/BF01078811

Jicha, B.R. and Hernández, W., 2021. Effusive and explosive eruptive history of the Ilopango caldera complex, El Salvador. *Journal of Volcanology and Geothermal Research*, p.107426. https://doi.org/10.1016/j.jvolgeores.2021.107426

Jones, T.J., Russell, J.K., 2017. Ash production by attrition in volcanic conduits and plumes. Sci. Rep. 7, 5538. https://doi.org/10.1038/s41598-017-05450-6

Koyaguchi, T., Woods, A.W., 1996. On the formation of eruption columns following explosive mixing of magma and surface water. J. Geophys. Res. 101, 5561-5574. https://doi.org/10.1029/95JB01687

Kutterolf, S., Freundt, A., Perez, W., Mörz, T., Schacht, U., Wehrmann, H., Schmincke, H.-U., 2008a. Pacific offshore record of plinian arc volcanism in Central America: 1. Along-arc correlations. Geochem. Geophys. Geosyst. 9,. https://doi.org/10.1029/2007GC001631

Kutterolf, S., Freundt, A., Perez, W., 2008b. Pacific offshore record of plinian arc volcanism in Central America: 2. Tephra volumes and erupted masses. Geochem. Geophys. Geosyst. 9,. https://doi.org/10.1029/2007GC001791

Lexa, J., Sebesta, J., Chávez, J.A., Hernández, W., Pecskay, Z., 2011. Geology and volcanic evolution in the southern part of the San Salvador Metropolitan Area. J. Geosci. 56, 106-140. http://dx.doi.org/10.3190/jgeosci.088

Lube, G., Breard, E.C., Esposti-Ongaro, T., Dufek, J. and Brand, B., 2020. Multiphase flow behaviour and hazard prediction of pyroclastic density currents. *Nature Reviews Earth & Environment*, *1*(7), pp.348-365. https://doi.org/10.1038/s43017-020-0064-8

Macedonio, G., Dobran, F. and Neri, A., 1994. Erosion processes in volcanic conduits and application to the AD 79 eruption of Vesuvius. *Earth and planetary science letters*, *121*(1-2), pp.137-152. https://doi.org/10.1016/0012-821X(94)90037-X

Mann, C.P., Stix, J., Vallance, J.W., Richer, M., 2004. Subaqueous intracaldera volcanism, Ilopango Caldera, El Salvador, Central America. Geol. Soc. Am. Spec. Pap. 375, 159-174.

Mastin, L.G., 2007. Generation of fine hydromagmatic ash by growth and disintegration of glassy rinds: J. Geophys. Res. 112, B02203. https://doi.org/10.1029/2005JB003883.

Mehringer, P.J., Sarna-Wojcicki, A.M., Wollwage, L.K., Sheets, P., 2005. Age and extent of the Ilopango TBJ tephra inferred from a Holocene chronostratigraphic reference section, Lago De Yojoa, Honduras. Quat. Res. 63, 199-205. https://doi.org/10.1016/j.yqres.2004.09.011

Meyer-Abich, H., 1956. Los volcanes actives de Guatemala y El Salvador. América Central. Anales del Servicio Geológico Nacional de El Salvador. Boletín N° 3. Ministerio de Obras Públicas, República de El Salvador. 102 pp.

Orsi, G., D'Antonio, M., de Vita, S., Gallo, G., 1992. The Neapolitan Yellow Tuff, a large-magnitude trachytic phreatoplinian eruption: eruptive dynamics, magma withdrawal and caldera collapse. J. Volcanol. Geotherm. Res. 53, 275-287. https://doi.org/10.1016/0377-0273(92)90086-S

Pedrazzi, D., Sunye-Puchol, I., Aguirre-Díaz, G., Costa, A., Smith, V.C., Poret, M., Dávila-Harris, P., Miggins, D.P., Hernández, W., Gutiérrez, E., 2019. The Ilopango Tierra Blanca Joven (TBJ) eruption, El Salvador: Volcano-stratigraphy and physical characterization of the major Holocene event of Central America. J. Volcanol. Geotherm. Res. 377, 81-102. https://doi.org/10.1016/j.jvolgeores.2019.03.006

Pittari, A., Cas, R.A.F. and Martí, J., 2005. The occurrence and origin of prominent massive, pumice-rich ignimbrite lobes within the Late Pleistocene Abrigo Ignimbrite, Tenerife, Canary Islands. *Journal of volcanology and geothermal research*, *139*(3-4), pp.271-293. https://doi.org/10.1016/j.jvolgeores.2005.10.007

Richer, M., Mann, C.P., Stix, J., 2004. Mafic magma injection triggers eruption at Ilopango caldera, El Salvador, Central America. Geol. Soc. Am. Spec. Pap. 375, 175-190.

Roche, O., 2015. Nature and velocity of pyroclastic density currents inferred from models of entrainment of substrate lithic clasts. *Earth and Planetary Science Letters*, *418*, pp.115-125. https://doi.org/10.1016/j.epsl.2015.03.001

Rose, W.I., Conway, F.M., Pullinger, C.R., Deino, A., McIntosh, W.C., 1999. An improved age framework for late Quaternary silicic eruptions in northern Central America. Bull. Volcanol. 61, 106-120. https://doi.org/10.1007/s004450050266

Sánchez-Esquivel, I.A., 2016. *Levantamiento batimétrico y medición de parámetros físicoquímicos en el Lago de Ilopango, El Salvador* (Doctoral dissertation, Thesis). Universidad de El Salvador. Recuperado a partir de http://ri. ues. edu. sv/10296).

Schumacher, R., Schmincke, H-U., 1991. Internal structure and occurrence of accretionary lapilli - a case study at Laacher See Volcano. Bull. Volcanol. 53, 612-634. https://doi.org/10.1007/BF00493689

Schumacher, R., Schmincke, H-U., 1995. Models for the origin of accretionary lapilli. Bull. Volcanol. 56, 626-639. https://doi.org/10.1007/BF00301467

Scott, A.C., Glasspool, I.J., 2005. Charcoal reflectance as a proxy for the emplacement temperature of pyroclastic flow deposits. Geology 33, 589-592. https://doi.org/10.1130/G21474.1

Self, S., 1983. Large-scale phreatomagmatic silicic volcanism: a case study from New Zealand. J. Volcanol. Geotherm. Res. 17, 433-469. https://doi.org/10.1016/0377-0273(83)90079-3

Self, S., Sparks, R.S.J., 1978. Characteristics of widespread pyroclastic deposits formed by the interaction of silicic magma and water. Bull. Volcanol. 41, 196-212. https://doi.org/10.1007/BF02597223

Sheets, P.D. (Ed), 1984. Archeology and Volcanism in Central America: The Zapotitán Valley of El Salvador. University of Texas Press, Austin, Texas, pp 151.

Sheets, P., 2004. Apocalypse then: social science approaches to volcanism, people, and cultures in the Zapotitan Valley, El Salvador. In: Rose, W.I., Bommer, J.J., Lopez, D.L., Carr, M.J., Major, J.J. (Eds) Natural Hazards in El Salvador. Geol. Soc. Am. Spec. Pap. 375, 109-120.

Smith, V.C., Costa, A., Aguirre-Díaz, G., Pedrazzi, D., Scifo, A., Plunkett, G., Poret, M., Tournigand, P.Y., Miles, D., Dee, M.W., McConnell, J.R., 2020. The magnitude and impact of the 431 CE Tierra Blanca Joven eruption of Ilopango, El Salvador. Proc. Natl. Acad. Sci. 117, 26061-26068. https://doi.org/10.1073/pnas.2003008117

Sparks, R.S.J. and Walker, G.P.L., 1977. The significance of vitric-enriched air-fall ashes associated with crystal-enriched ignimbrites. *Journal of Volcanology and Geothermal Research*, *2*(4), pp.329-341. https://doi.org/10.1016/0377-0273(77)90019-1

Sparks, R.S.J., Wilson, L., Sigurdsson, H., 1981. The pyroclastic deposits of the 1875 eruption of Askja, Iceland. Phil. Trans. R. Soc. Lond. A299, 241-273. https://doi.org/10.1098/rsta.1981.0023

Stoiber, R. and Carr, M., 1973. Quaternary volcanic and tectonic segmentation of Central America. *Bulletin Volcanologique*, *37*(3), pp.304-325.

Sulpizio, R., Dellino, P., Doronzo, D.M. and Sarocchi, D., 2014. Pyroclastic density currents: state of the art and perspectives. *Journal of Volcanology and Geothermal Research*, *283*, pp.36-65. https://doi.org/10.1016/j.jvolgeores.2014.06.014

Suñe-Puchol, I., Aguirre-Díaz, G.J., Pedrazzi, D., Dávila-Harris, P., Miggins, D.P., Costa, A., Ortega-Obregón, C., Lacan, P., Gutierrez, E., Hernández, W., 2019a. The Ilopango caldera complex, El

Salvador: Stratigraphic revision of the complete eruptive sequence and recurrence of large explosive eruptions. J. Volcanol. Geotherm. Res. 371, 100-119. https://doi.org/10.1016/j.jvolgeores.2019.02.011

Suñe-Puchol, I., Aguirre-Díaz, G.J., Dávila-Harris, P., Miggins, D.P., Pedrazzi, D., Costa, A., Ortega-Obregón, C., Lacan, P., Hernández, W., Gutiérrez, E., 2019b. The Ilopango caldera complex, El Salvador: Origin and early ignimbrite-forming eruptions of a graben/pull-apart caldera structure. J. Volcanol. Geotherm. Res. 371: 1-19. https://doi.org/10.1016/j.jvolgeores.2018.12.004

Taddeucci, J., Scarlato, P., Montanaro, C., Cimarelli, C., Del Bello, E., Freda, C., Andronico, D., Gudmundsson, M.T., Dingwell, D.B., 2011. Aggregation-dominated ash settling from the Eyjafjallajökull volcanic cloud illuminated by field and laboratory high-speed imaging. Geology 39, 891-894. https://doi.org/10.1130/G32016.1

Van Eaton, A.R., Herzog, M., Wilson, C.J.N., McGregor, J., 2012a. Ascent dynamics of large phreatomagmatic eruption clouds: The role of microphysics. J. Geophys. Res. 117, B03203, https://doi.org/10.1029/2011JB008892

Van Eaton, A.R., Muirhead, J.D., Wilson, C.J.N., Cimarelli, C., 2012b. Growth of volcanic ash aggregates in the presence of liquid water and ice: an experimental approach. Bull. Volcanol. 74, 1963-1984. https://doi.org/10.1007/s00445-012-0634-9

Van Eaton, A.R., Wilson C.J.N., 2013a. The nature, origins and distribution of ash aggregates in a large-scale wet eruption deposit: Oruanui, New Zealand. J. Volcanol. Geotherm. Res. 250, 129-154. https://doi.org/10.1016/j.jvolgeores.2012.10.016

Van Eaton, A.R., Harper, M.A., Wilson, C.J.N., 2013b. High-flying diatoms: Widespread dispersal of microorganisms in an explosive volcanic eruption. Geology 41, 1187-1190. https://doi.org/10.1130/G34829.1

Van Eaton, A.R., Mastin, L.G., Herzog, M., Schwaiger, H.F., Schneider, D.J., Wallace, K.L. and Clarke, A.B., 2015. Hail formation triggers rapid ash aggregation in volcanic plumes. *Nature communications*, *6*(1), pp.1-7. https://doi.org/10.1038/ncomms8860

Walker, G.P.L., 1981. Characteristics of two phreatoplinian ashes, and their water-flushed origin. J. Volcanol. Geotherm. Res. 9, 395-407. https://doi.org/10.1016/0377-0273(81)90046-9

Whelley, P.L., Calder, E.S. and Wooller, L., 2017. The emplacement dynamics of pumice lobes ascertained from morphology and granulometry: Examples from the 1993 deposits at Lascar Volcano, Chile. *Journal of Volcanology and Geothermal Research*, *342*, pp.79-90. https://doi.org/10.1016/j.jvolgeores.2017.06.015

Wilson, C.J.N., 2001. The 26.5 ka Oruanui eruption, New Zealand: an introduction and overview. J. Volcanol. Geotherm. Res. 112, 133-174. https://doi.org/10.1016/S0377-0273(01)00239-6

Supplementary File 1. Excel spreadsheet with latitude and longitude coordinates for localities visited in this study.

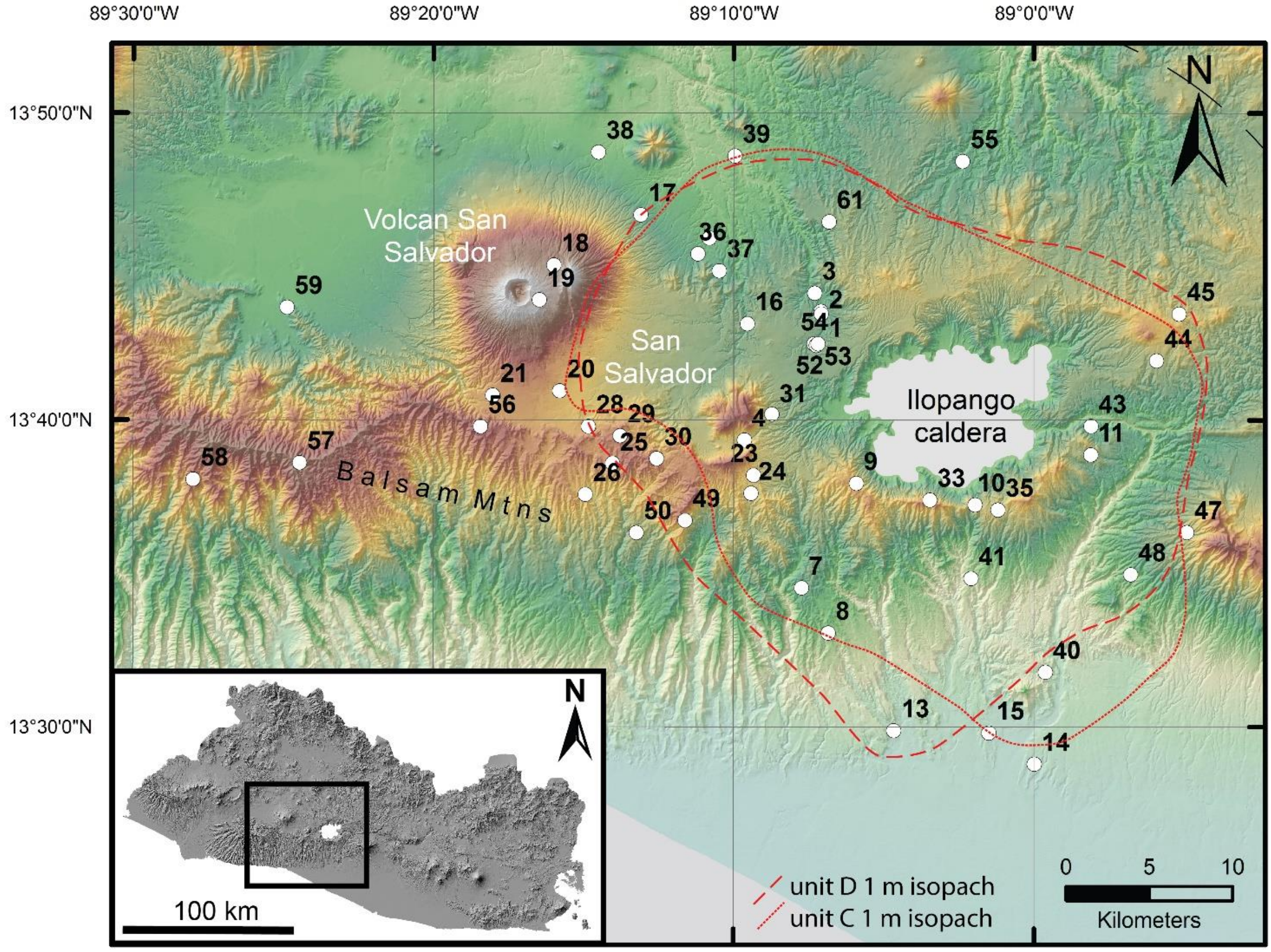


Figure 1. Location maps. (a) Digital terrain model of Ilopango volcano and surroundings showing location of measured sections of units C and D, labelled with locality ID number. Red lines show 1-m isopachs for total thickness of units C (solid) and D (dashed). Black dashed lines represent ultra-proximal (<10 km), proximal (10–15 km), and medial zones (15–25 km) around the caldera. Distances beyond 25 km are distal for the purposes of this study. [2 column]

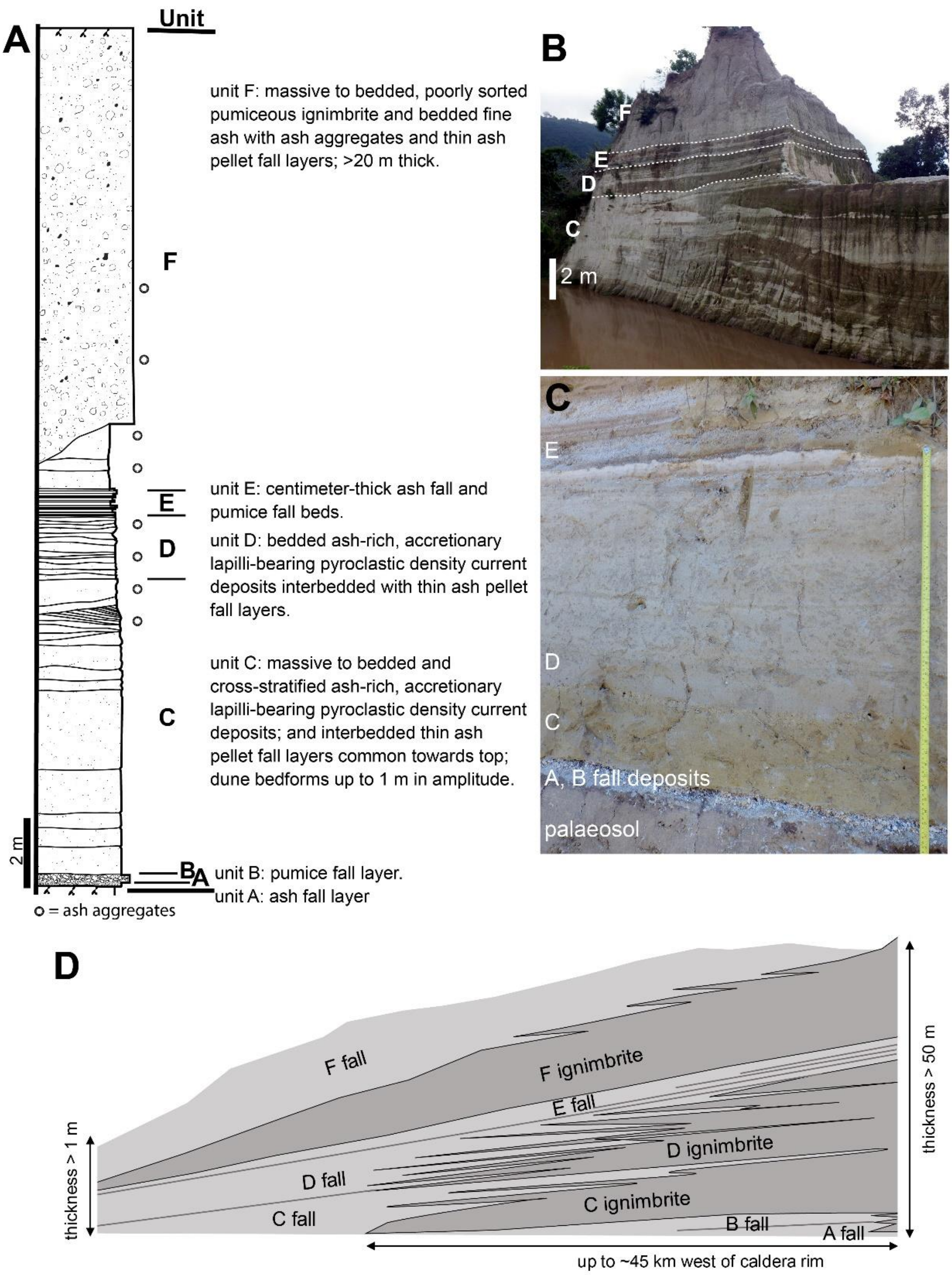


**Figure 2.** The TBJ stratigraphy. (a) General vertical section of the TBJ eruption deposits. (b) Units C-F at locality 4 km west of the caldera centre featured in Figure 2a (refer to Fig. 1). Lower left of photo shows large dune bedforms of unit C. (c) Distal outcrop of units A-E (locality 17). Measuring tape is extended 1 m. Unit G (not shown) is the coignimbrite fall deposit associated with unit F pyroclastic

density currents. D. Schematic diagram of the stratigraphic relationships of the ignimbrite and fall deposit units of the TBJ eruption. [2 column]

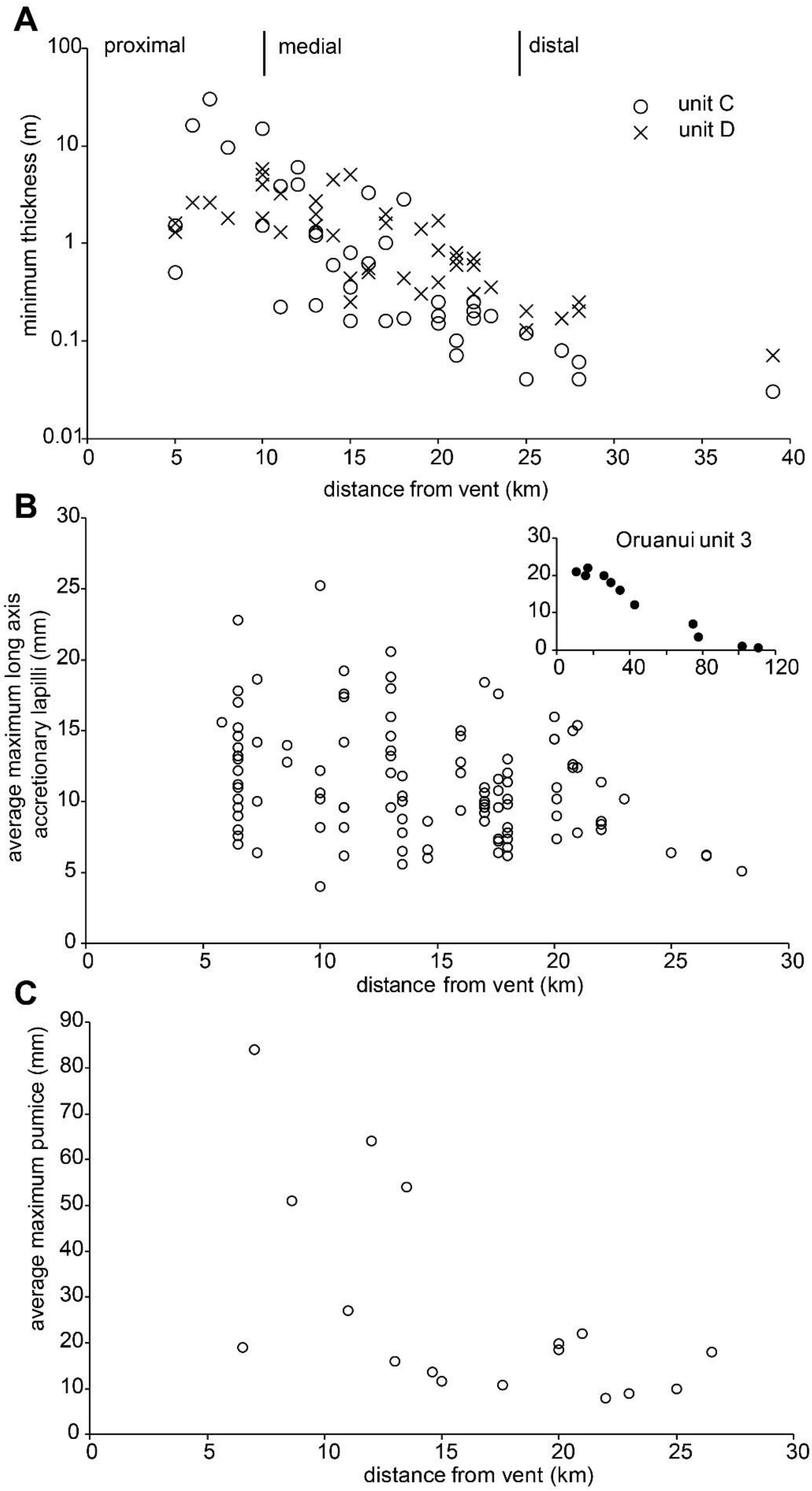


**Figure 3.** Thickness and clast size data. (a) Thickness data for units C and D pyroclastic density current deposits plotted against distance from centre of Lake Ilopango. Clast size variation with distance. (b)

Average long axes accretionary lapilli plotted against distance from caldera center for unit D. Values are averages of the long axes from the five largest accretionary lapilli in a single bed. Note general decrease in absolute maximum diameter with distance from source. Inset shows corresponding data (same axes) from unit 3 of the 25.4 ka Oruanui eruption, New Zealand, from Van Eaton and Wilson (2013a). (c) Maximum pumice (average long axis of five largest clasts) for Unit C. [1.5 column]

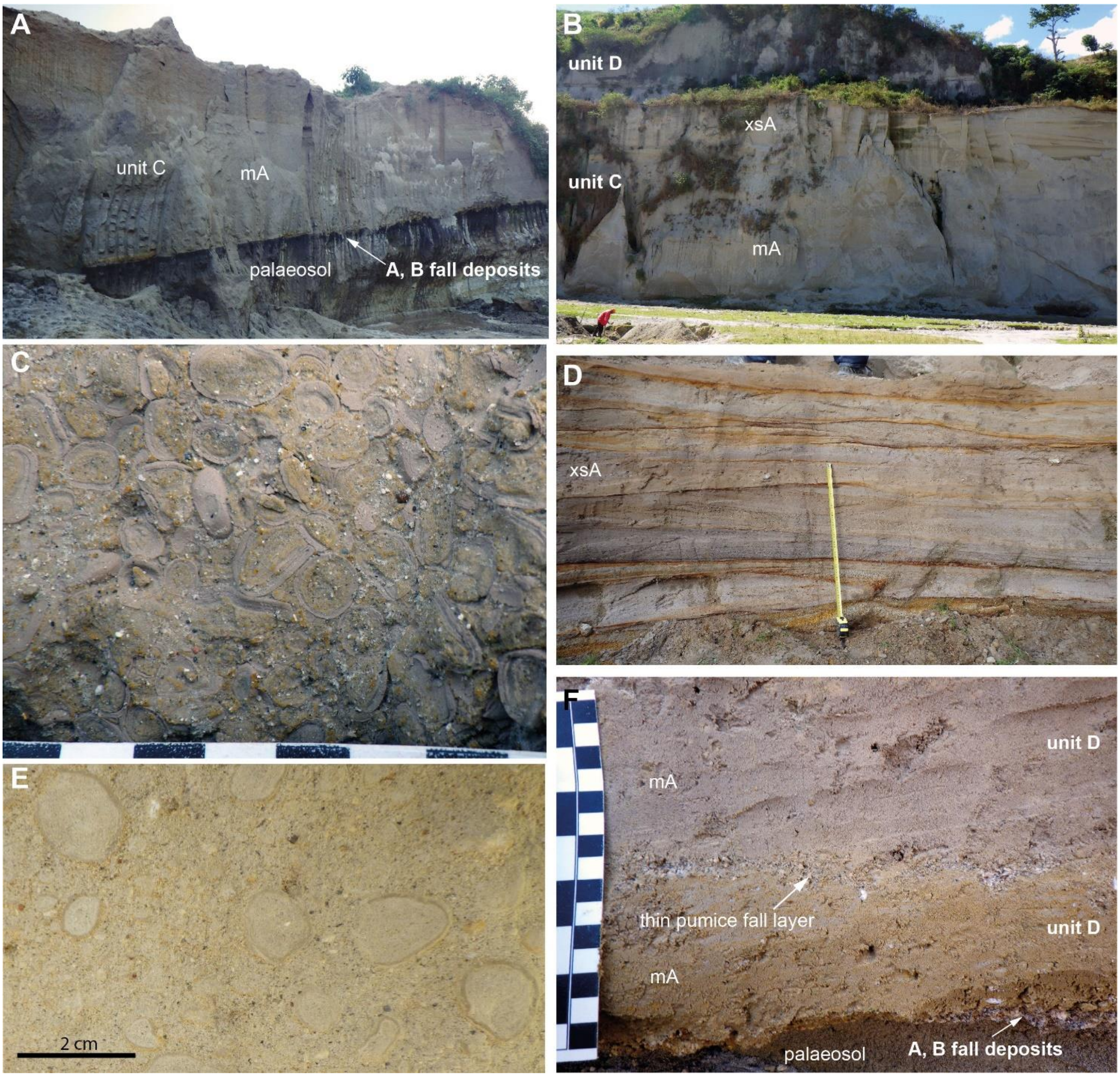


**Figure 4.** Unit C of the TBJ. (a) Basal contact in quarry (locality 4). Deposits thicken into shallow paleovalley. (b) Thick outcrop with well developed, large amplitude dune bedforms in upper centre (locality 1). Cliff is ~15 m high. (c) Large, clast-supported accretionary lapilli in Unit C on southeast margin of caldera (locality 35). Scale shows 1 cm divisions. (d) Cross-stratified deposits east of caldera (locality 44). Current from left to right. 50 cm on tape measure. (e) Matrix-supported accretionary lapilli (Locality 31). (f) Thin pumice fall layer (white clasts) separating units C and D (Locality 14). Scale shows 1 cm divisions. [2 column]

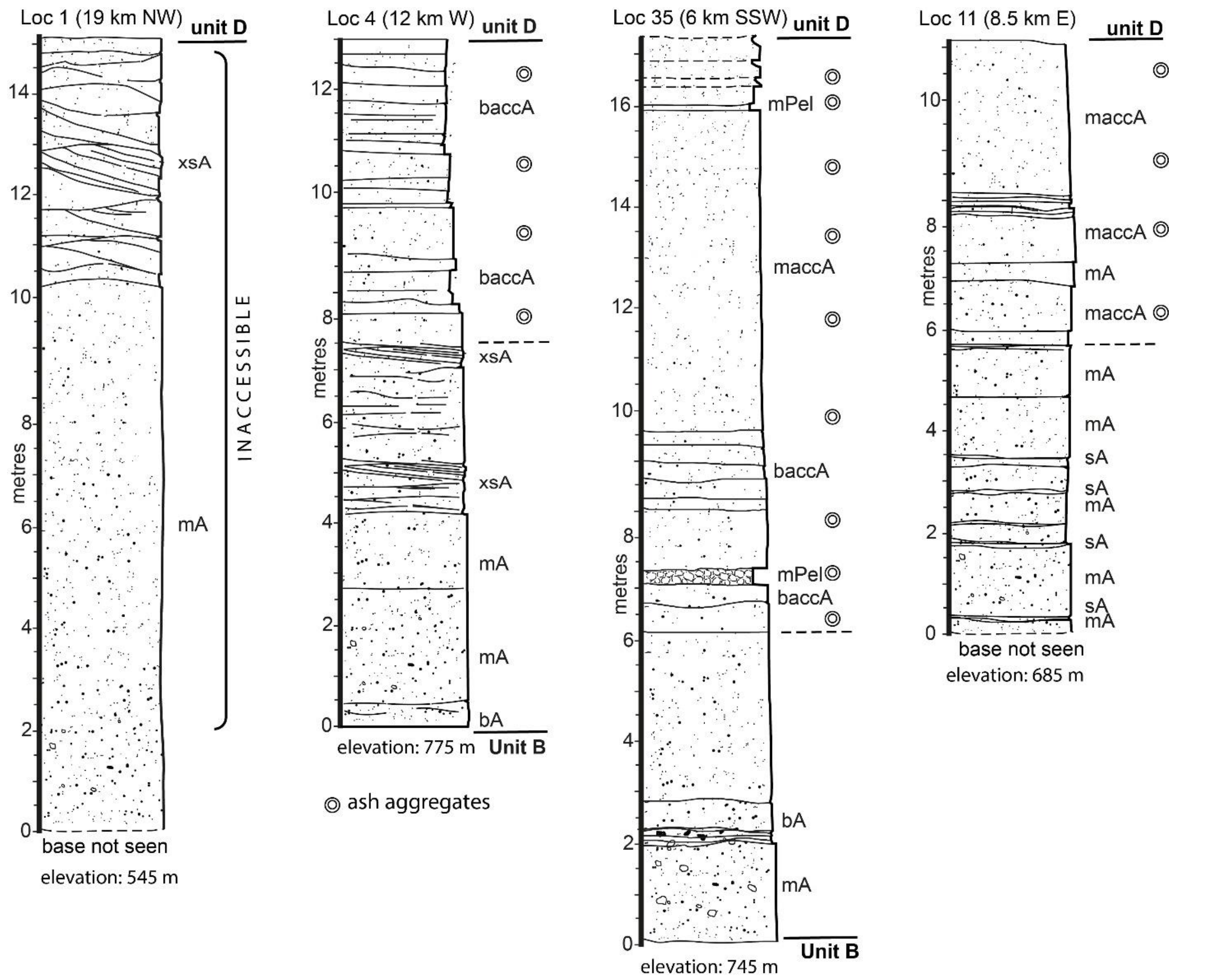


**Figure 5.** Measured sections through thick proximal outcrops of unit C. Note base is not exposed at Localities 1 and 11. See Figure 1 for location of measured sections. Lithofacies explanations given in Table 1. [2 column]

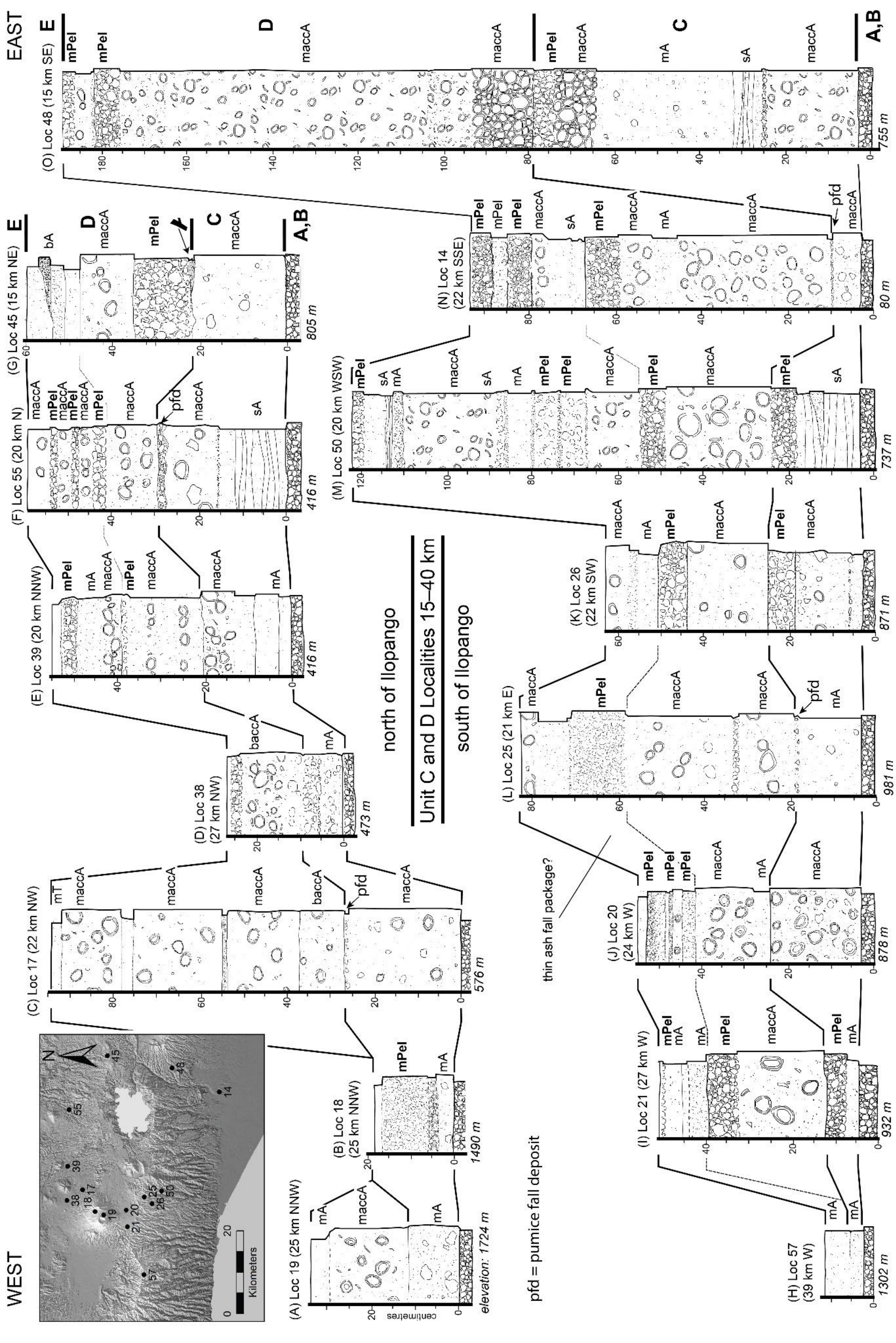
WEST
EAST
Unit C and D Localities 15–40 km
north of Ilopango
south of Ilopango
pfd = pumice fall deposit
thin ash fall package?
Kilometers
0
20
(A) Loc 19 (25 km NNW)
elevation: 1724 m
centimetres
(B) Loc 18 (25 km NNW)
1490 m
(C) Loc 17 (22 km NW)
576 m
(D) Loc 38 (27 km NW)
473 m
(E) Loc 39 (20 km NNW)
416 m
(F) Loc 55 (20 km N)
416 m
(G) Loc 45 (15 km NE)
805 m
(H) Loc 57 (39 km W)
1302 m
(I) Loc 21 (27 km W)
932 m
(J) Loc 20 (24 km W)
878 m
(L) Loc 25 (21 km E)
981 m
(K) Loc 26 (22 km SW)
871 m
(M) Loc 50 (20 km WSW)
737 m
(N) Loc 14 (22 km SSE)
80 m
(O) Loc 48 (15 km SE)
755 m
mA
maccA
baccA
sA
bA
mPel
mT
pfd
A,B
C
D
E

**Figure 6.** Measured sections though units C and D. Lithofacies explanations given in Table 1. pfd = thin pumice fall deposit between units C and D. [2 column]

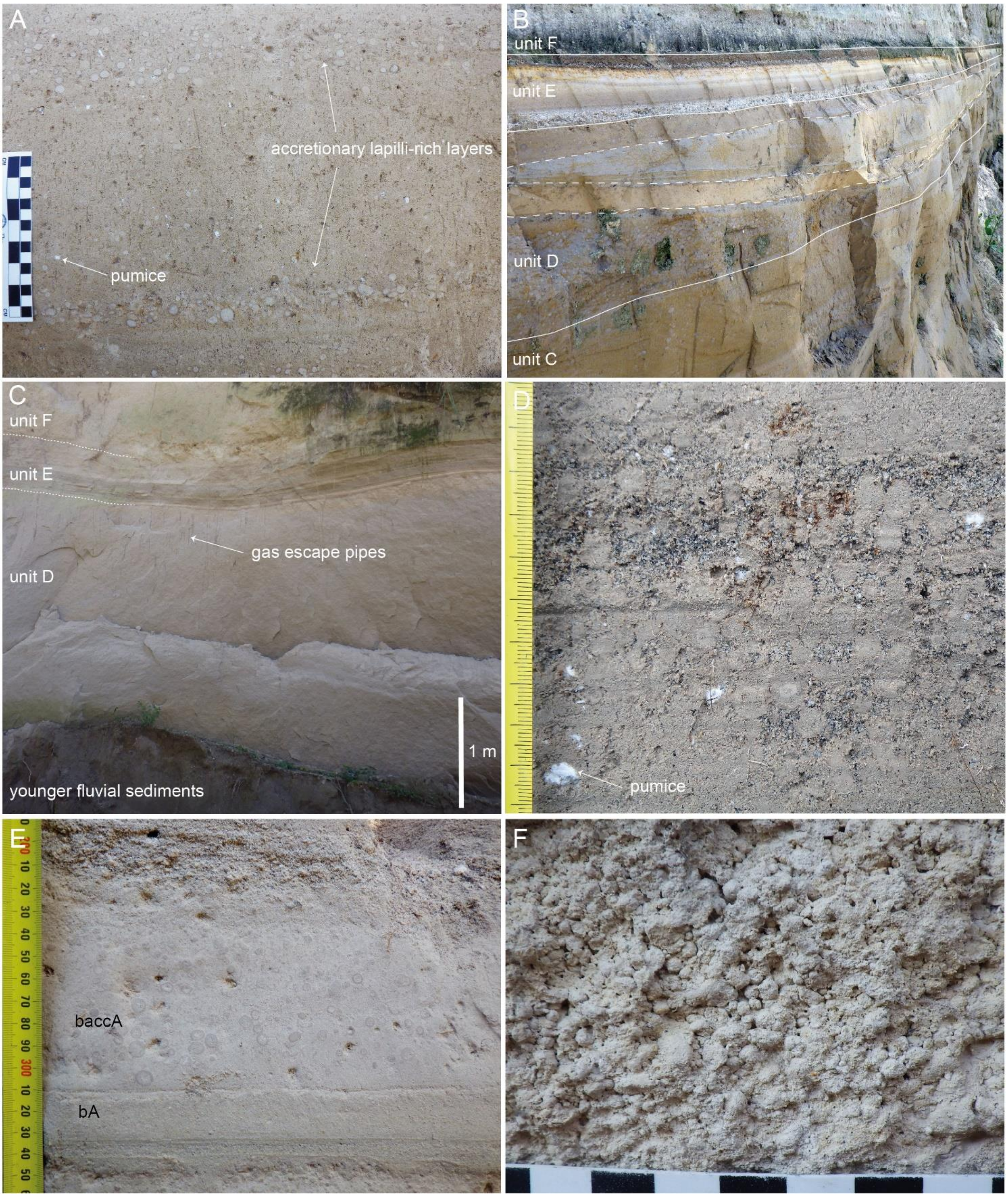

**Figure 7.** Unit D of the TBJ. A) Typical accretionary lapilli-rich deposit (lithofacies maccA, Table 1) (locality 4). Stratification is defined by variations in the abundance of accretionary lapilli. Smallest divisions on scale are centimetres. B) Lenticular beds of lithofacies maccA (Table 1). (Locality 27). 1.5 m of deposit units C and D shown. C) PDC deposit with elutriation pipes found only in ultra-proximal zone on NE of caldera (Locality 52). D) Fines-depleted, accretionary lapilli-bearing lithofacies (lithofacies fdaccA, Table 1) (locality 9). 1 cm divisions on scale. E) Thinly bedded ash beds at top of unit D (Locality 61). Beds are defined by variations in abundance of ash aggregates and by bedding planes. Ruler shows millimetres. F) Clast-supported ash pellet fall layer (lithofacies mPel, Table 1) (Locality 15). Scale shows 1 cm divisions. [2 column]

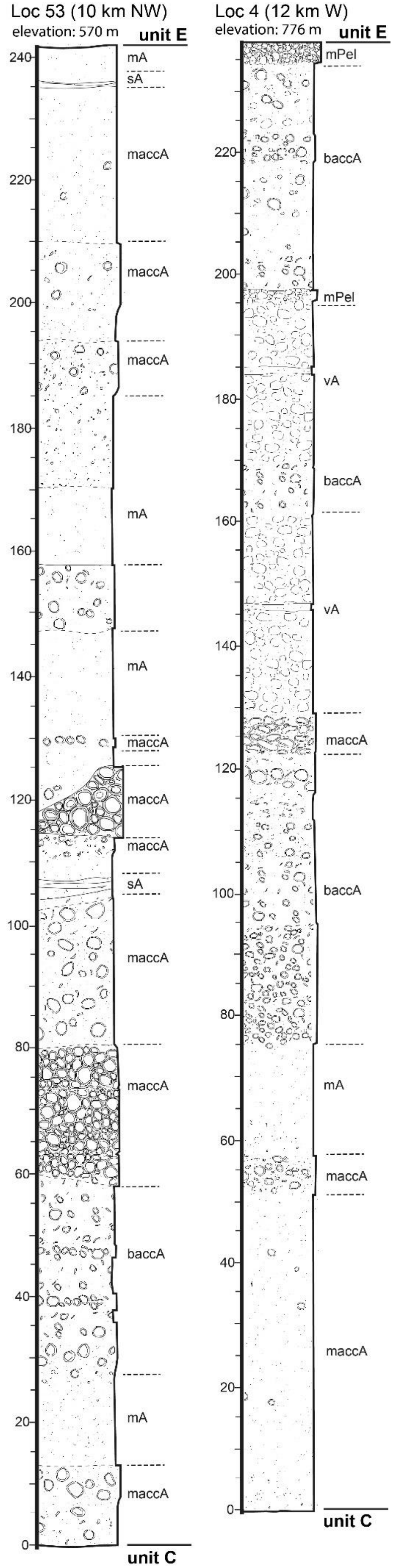

Loc 53 (10 km NW)
elevation: 570 m
unit E
mA
sA
maccA
maccA
maccA
mA
mA
maccA
maccA
maccA
sA
maccA
maccA
baccA
mA
maccA
unit C
Loc 4 (12 km W)
elevation: 776 m
unit E
mPel
baccA
mPel
vA
baccA
vA
maccA
baccA
mA
maccA
maccA
unit C


855

**Figure 8.** Measured sections through thick proximal sections of unit D. See Figure 1 for locations. Lithofacies explanations given in Table 1. [1 column]

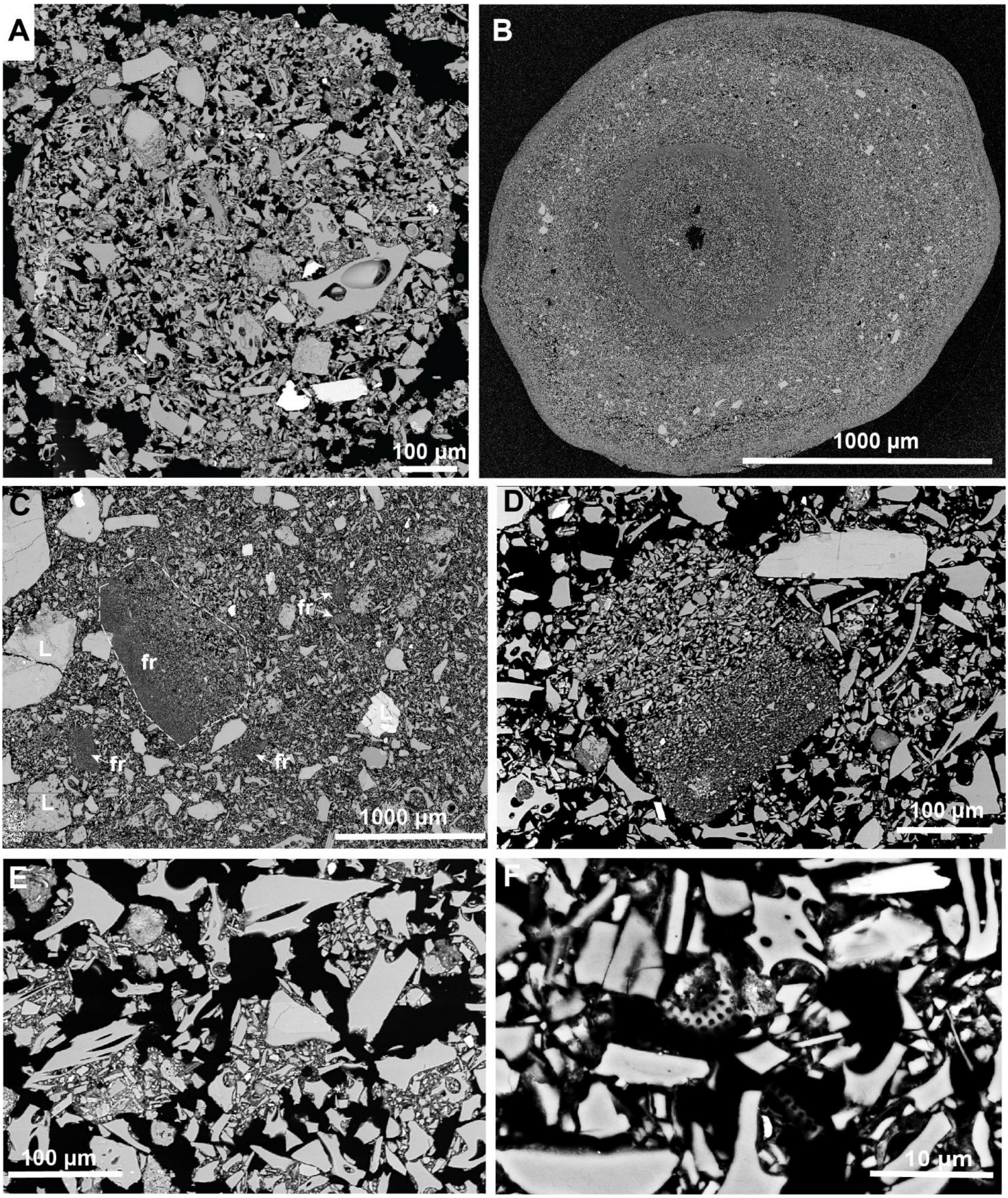

**Figure 9.** Backscattered SEM images of ash aggregates in TBJ PDC deposits. (a) Small, unstructured ash pellet in mPel layer. (b) AP2 aggregate showing multiple concentric layers of texturally-distinct ash and a central vacuole which may have originally hosted an ice nucleus (c.f. Van Eaton et al., 2012b). (c) and (d) Fragments of accretionary lapilli in Unit D matrix. Fr= fragments, L = lithic clast. (e) Matrix of massive accretionary lapilli-bearing ash in Unit D is composed of small ash clusters. (f). Diatom in outer rim of an accretionary lapilli in Unit D. [2 column]

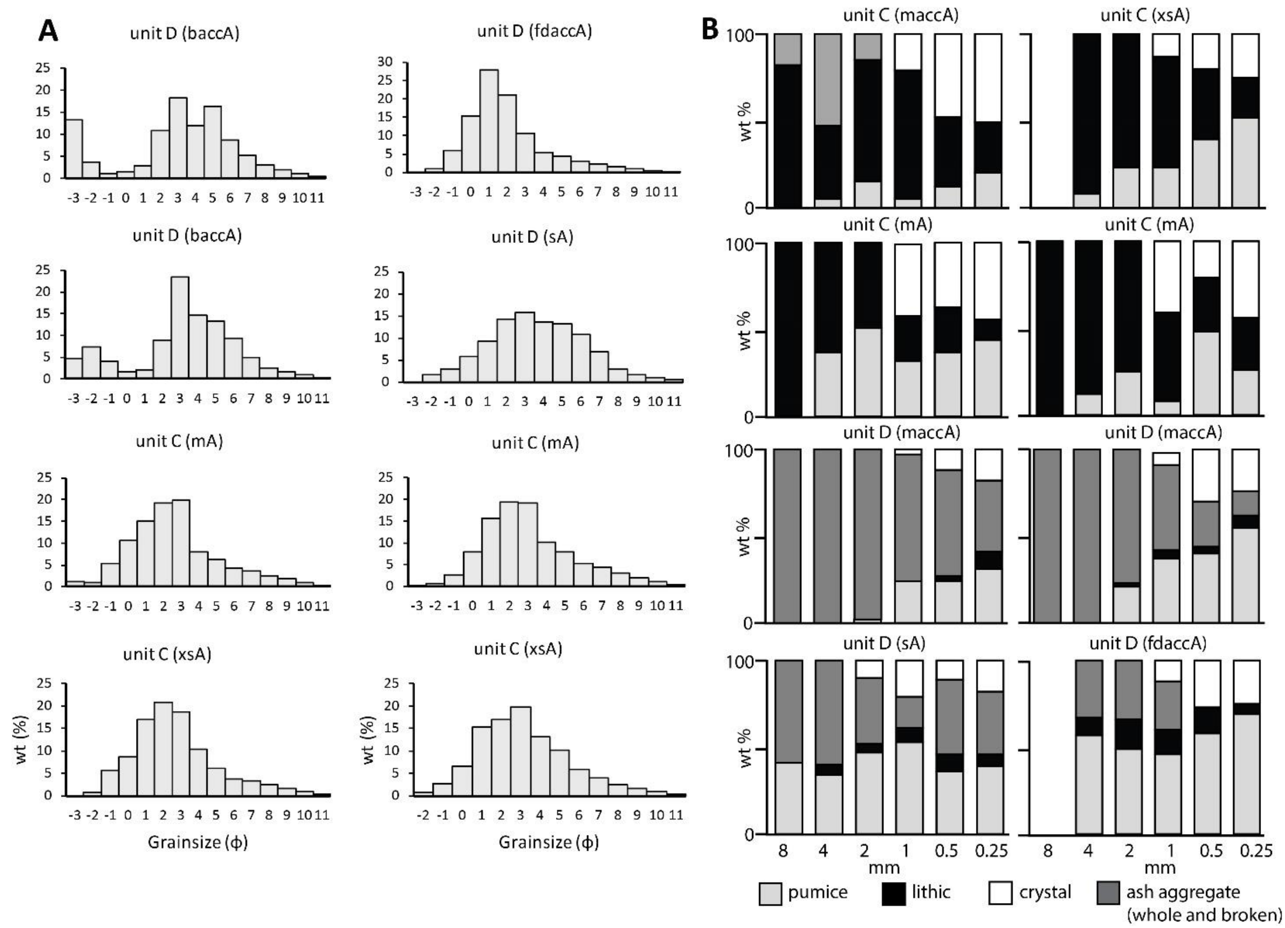


**Figure 10.** Histograms of particle size distributions for the representative lithofacies in units C and D. Care was taken during sieving to keep whole and broken ash aggregates intact. B) Componentry data for representative lithofacies from units C and D. See table 1 for lithofacies terms. Coarse tail is dominated by lithic clasts in unit C and accretionary lapilli (AP2 ash aggregates) in unit D [3 column]

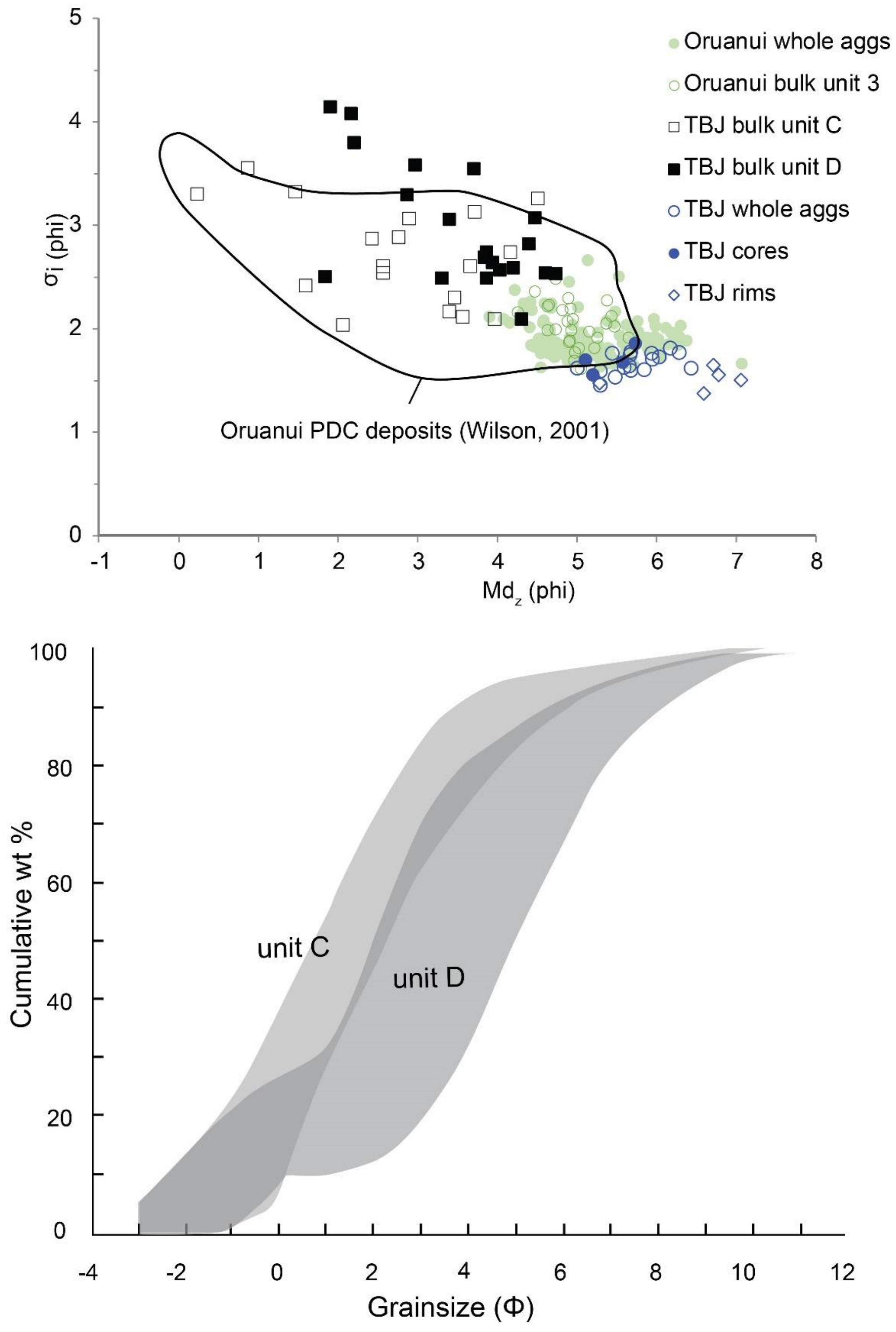


**Figure 11.** Grainsize characteristics of TBJ units C and D. (a) Median diameter ($Md_{\varphi}$,, defined as the 50$^{th}$ percentile) vs sorting (inclusive graphic standard deviation, $\sigma_i$), calculated as in Folk and Ward (1957) are plotted for bulk pyroclastic density current deposit samples, and individual crushed

aggregates, cores, and rims from unit D . Grain size data from the Oruanui eruption of Taupo, New Zealand, are plotted for comparison (from supplementary data of Van Eaton and Wilson, 2013a), along with the fall and pyroclastic density current fields of Walker (1981). (b) Cumulative frequency graphs of grainsize distributions for units C and D (26 samples). [1.5 column]

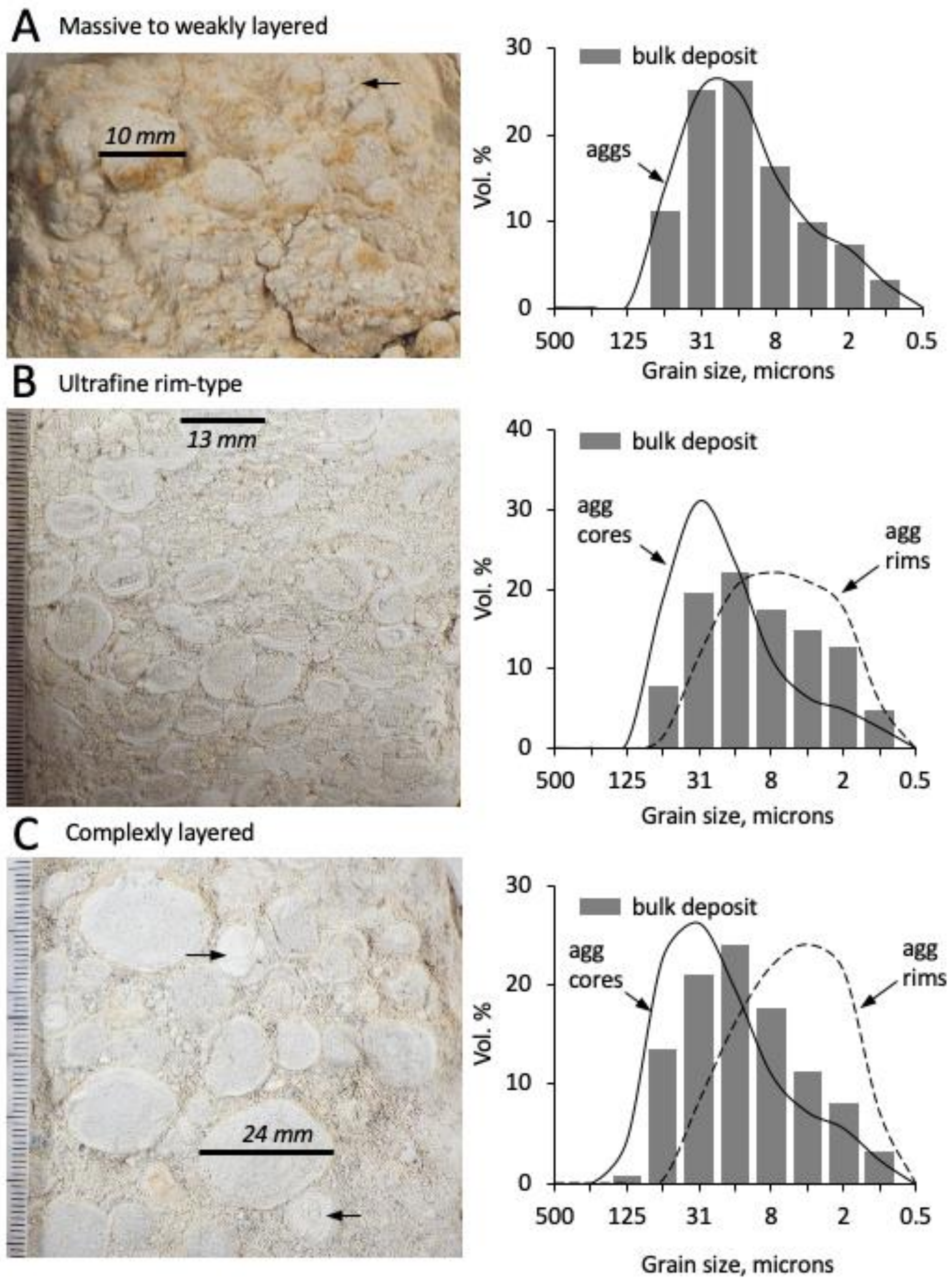

**Figure 12.** Examples from TBJ unit D showing photographs of different aggregate textures (left) and corresponding grain size data (right). Photos show dried bulk samples blasted with compressed air to reveal details. (a) Clast-supported fall bed of massive to weakly layered ash pellets from locality 27 (sample 46a). Arrow points to a weakly layered aggregate in the photo. The grain size of the bulk deposit (grey bars) from this bed is nearly identical to that of its individual, crushed aggregates (black curve). (b) Pyroclastic density current facies containing clast-supported, ultrafine rim-type accretionary lapilli from locality 35 (sample 62). Note the consistent transition from coarser core to finer rim, with a substantial outer layer (2-3 mm) rich in ultrafine ash <10 um. (c) Pyroclastic density current facies containing complexly layered accretionary lapilli from locality 50 (sample 95). These aggregates haver larger diameters, a relatively thin outermost rim (~1 mm), and complicated growth histories, including repeating layers of coarser and finer ash (arrows), indicating multiple cycles of re-entrainment. Note how in (b) and (c) the aggregates and fragments are generally surrounded by fine matrix, but nearly clast-supported in places. [1.5 column]

Supplementary File 1. Excel spreadsheet with latitude and longitude coordinates for localities visited in this study.

Table 1. Summary description and interpretation of lithofacies in units C and D of the TBJ eruption.

| **Lithofacies name and code** | **Lithology** | **Md (φ)** | **Sorting (σφ)** | **Structure and geometry** | **Occurrence** | **Interpretation** |
|---|---|---|---|---|---|---|

| | | | | | | |
|---|---|---|---|---|---|---|
| Massive ash (mA) | Ash with minor lithic and angular pumice lapilli clasts (<1–5 wt. %) | 1–2.8 | 1.95–3 | Beds cm-dm thick; thicken and thin laterally | C and D: proximal to medial areas | pyroclastic density current deposit |
| Bedded ash (bA) | As mA | | | As mA; beds 1–50 cm thick; beds subparallel or thicken and thin | C and D: proximal to distal areas | pyroclastic density current deposit |
| Cross-stratified / stratified ash (xsA/sA) | Fine to coarse ash with 2–15 wt. % pumice and lithic clasts | 1.9–3 | 2–3.85 | Strata mm-cm thick; occurs in packages up to several 10s cm thick (D) or several meters thick (C); laterally continuous over 10s–100s m; thicken and thin laterally | D proximal to distal areas. | Traction sedimentation from a fully dilute pyroclastic density current |
| Massive / bedded ash with accretionary lapilli (maccA / baccA) | As mA/bA; contains whole and broken accretionary lapilli ([1]AP2) in concentrations up to 70 wt. % | 0.9–4.4 | 2.3–3.75 | Accretionary lapilli occur dispersed throughout or in discontinuous layers and lenses; packages up to several metres thick; individual | C: upper parts in proximal to distal areas D: throughout; | pyroclastic density current deposit; accretionary lapilli fell in from suprajacent ash |

| | | | | | | |
|---|---|---|---|---|---|---|
| | | | | beds thicken and thin | proximal to distal. | clouds and were transported by the current |
| Massive ash pellets (mpel) | Clast-supported ash pellets ([2]AP1) and ash clusters ([3]PC1) | - | - | Occurs in beds typically 1–5 cm thick; generally continuous across outcrops | C: medial and distal areas D: proximal to distal areas; more common in distal areas | Fall deposit from co-ignimbrite plumes or eruption plume-fed ash cloud |
| Vesicular ash (vA) | Massive ash with subspherical vesicles | - | - | Beds 2–5 cm thick; beds persistent across outcrops | D: proximal to distal area | Coalesced wet ash pellet fall layers |
| Fines-depleted ash with accretionary lapilli (fdaccA) | Whole and broken accretionary lapilli in a matrix of fines-depleted coarse lithic-crystal-pumice ash | 1–2 | 1.9–2.6 | Centimetre-scale lenses and cm-scale pockets | D: proximal areas | Elutriation zones in pyroclastic density current deposits driven by water vapour |

[1]concentrically structured accretionary pellets; [2]poorly structured accretionary pellets; [3]particle clusters; terminology from Brown et al., (2012)